Journal of Geophysical Research, accepted 2009 May 28, doi:10.1029/2009JD011760

Analysis of tropical tropospheric ozone, carbon monoxide and water vapor during the 2006 El Niño using TES observations and the GEOS-Chem model

Ray Nassar,[1,2] Jennifer A. Logan,[1] Inna A. Megretskaia,[1] Lee T. Murray,[1] Lin Zhang,[3] and Dylan B. A. Jones[4]

[1] School of Engineering and Applied Sciences, Harvard University

[2] now at Departments of Physics and Geography, University of Toronto

[3] Department of Earth and Planetary Science, Harvard University

[4] Department of Physics, University of Toronto

Abstract

Elevated levels of tropical tropospheric ozone (O_3) and carbon monoxide (CO), and decreased water (H_2O) vapor were observed by the Tropospheric Emission Spectrometer (TES) in the region of Indonesia and the eastern Indian Ocean during the coincident positive phases of the El Niño Southern Oscillation (ENSO) and Indian Ocean Dipole (IOD) in late 2006. Using the chemical transport model GEOS-Chem, we show that the elevated CO results from increased biomass burning in Indonesia during the ENSO/IOD-induced drought, and quantify the effect of the fires and other factors on O_3. In the region of highest CO (~200 ppb), the contribution of the fires to enhanced O_3 is ~45% in October, ~75% in early November, and only 10% in December. More lightning in late 2006 compared to 2005 causes an increase in O_3 of a few ppb. Dynamical changes increase O_3 over a larger region than fire emissions which mainly increase O_3 at 10ºN-10ºS in October and November. The model matches the O_3 anomaly in October, but underestimates it in November and December, which we ascribe to overly active convection in the model in late 2006, based on an analysis of Outgoing Longwave Radiation (OLR) data. An underestimate of NO_x emissions from soils may also contribute to the disparity at the end of the year. A dramatic decrease in O_3 in late 2006 in equatorial Africa and the western Indian Ocean is reproduced by the model and is caused by highly enhanced convection in 2006, likely associated with the IOD.

1. Introduction

The El Niño Southern Oscillation (ENSO) is a coupled oceanic-atmospheric mode of interannual variability in the Earth system. During the positive phase of ENSO, known as El Niño, sea surface temperatures (SSTs) in the equatorial central Pacific Ocean are persistently higher than normal and are accompanied by changes in ocean currents and surface winds. These changes increase atmospheric convection and humidity over the western Pacific with a corresponding decrease over Indonesia, its neighboring islands and the eastern Pacific [*Bjerknes*, 1969; *Rasmusson and Wallace*, 1983]. Through this shift in convection, ENSO affects precipitation, which leads to changes in soil moisture, vegetation growth rates, and the distribution and rate of biomass burning. The impact of El Niño is especially strong for coastal areas of the tropical western Pacific, with the most severe effects experienced in Indonesia, which can lead to large scale changes in the chemical composition of the atmosphere.

An intercomparison of climate models suggests that contemporary El Niño conditions in the tropics may provide an example of the anthropogenically-induced climate warming that will occur in the future [*Yamaguchi and Noda*, 2006]. Other studies show a strong link between ENSO and the highly variable rate of tropospheric carbon dioxide (CO_2) accumulation [*Bacastow*, 1976; *Keeling et al.*, 1995; 2001; *Heimann and Reichstein*, 2008], with some suggesting that a key mechanism for this variability is the enormous release of CO_2 due to biomass burning that occurs in Indonesia during El Niño [*Langenfelds et al.*, 2002; *Page et al.*, 2002].

The effects of ENSO on atmospheric chemistry, and tropospheric O_3 in particular, have been investigated using both measurements and models. The earliest work used tropospheric O_3 columns derived from satellite observations [*Ziemke and Chandra*, 1998; *Chandra et al.*, 1998]. These studies analyzed anomalies of O_3, H_2O vapor and Outgoing Longwave Radiation (OLR) for the strong 1997 El Niño (computed as the difference between these parameters in the El Niño year and a baseline year) and found that high O_3 over Indonesia correlated with low H_2O vapor and low convection, while low O_3 over the Pacific correlated with high H_2O vapor and high convection. The spatial patterns of change in O_3, H_2O and OLR are referred to as 'asymmetric dipole anomalies'. Enhanced O_3 during El Niño was also evident in ozonesonde profiles from Indonesia [*Fujiwara et al.*, 1999; *Kita et al.*, 2000]. Early modeling studies of the tropospheric chemistry associated with ENSO [*Hauglustaine et al.*, 1999; *Sudo and Takahashi*, 2001; C*handra et al.*, 2002] along with an observation-based study [*Thompson et al.*, 2001] all concluded that enhanced tropospheric O_3 during the 1997 El Niño was caused by a combination of biomass burning and tropospheric dynamics. *Duncan et al.* [2003a] investigated the impact of the 1997 Indonesian wildfires on atmospheric composition using the GEOS-Chem model, as well as the contribution to O_3 from NO_x produced by lightning.

The ENSO-induced drought which occurs on the islands of Indonesia makes this region globally unique in terms of the extreme degree of interannual variability in biomass burning [*Duncan et al.*, 2003b]. While the burning of above-ground vegetation makes a significant contribution to emissions from Indonesia, a larger contribution comes from burning of the thick layer of peat comprising the forest floor [*Levine*, 1999]. Although most biomass burning is the deliberate result of human activity (primarily to clear land for agriculture), high levels of burning are only

possible during periods of prolonged drought, thus natural drivers of tropospheric chemical variability in the region are difficult to separate from human influence. The level of biomass burning in Indonesia during the 1997 El Niño was the most extreme for that region ever recorded [*Duncan et al.*, 2003b], in part because the *Mega Rice Project* promoted by the Indonesian government from 1995-1999 involved drainage of large areas of peatlands in an unsuccessful attempt to introduce intense rice farming to southern Kalimantan on the island of Borneo [*Page et al.*, 2002; *Aldhous et al.*, 2004]. Without this large-scale unsustainable land use prior to the 1997 drought, the degree of burning at the time would likely not have been as severe, although *Field and Shen* [2008] showed that the probability of extreme biomass burning in Indonesia is not represented by a gradual change, but abruptly increases when precipitation drops below a threshold value.

In autumn 2006, the western and central tropical Pacific just north of the equator were wetter than normal, while Indonesia was much drier [*van der Werf et al.*, 2008], which is consistent with past El Niño conditions [*Chandra et al.*, 1998; 2007]. The positive phase of the Indian Ocean Dipole (IOD) [*Saji et al.*, 1999] also correlates with drought in areas surrounding the Indian Ocean. Although ENSO's impact on Indonesian precipitation is larger than that of the IOD, Indonesian drought and biomass burning are possibly most intense when the positive phases of ENSO and IOD coincide, which has only occurred 4 times in the past 50 years, including autumn 1997 [*Saji et al.*, 1999; *Thompson et al.*, 2001] and 2006 [*Field and Shen*, 2008]. The second highest level of CO emission from Indonesia reported in biomass burning inventories occurred in 2006 [*van der Werf et al.*, 2008], surpassed only by 1997. Satellite observations of tropospheric CO are not available for 1997, but observations in 2006 by multiple instruments [*Logan et al.*, 2008; *Rinsland et al.*, 2008; *Yurganov et al.*, 2008; also *http://web.eos.ucar.edu/mopitt/*] show the highest level of tropospheric CO in the satellite record for this region.

In the present work, we investigate tropospheric CO, O_3, and H_2O based on observations by the Tropospheric Emission Spectrometer (TES) [*Beer*, 2006] during the El Niño and positive IOD in late 2006, by contrasting to 2005, which was a neutral year with respect to ENSO. TES observations have sufficient vertical resolution, spatial and temporal coverage, accuracy and precision for detailed studies of tropospheric chemistry and transport. These simultaneous coincident measurement of CO, O_3, and H_2O from TES provide an advantage relative to many earlier studies of O_3 during El Niño, since CO is a more direct proxy for biomass burning than aerosols, which were used in the past [*Thompson et al.*, 2001; *Chandra et al.*, 2002]. *Logan et al.* [2008] identified strong anomalies in TES CO, O_3, and H_2O during October and November of 2006. Using TES observations and the GEOS-Chem model [*Bey et al.*, 2001], we investigate the effects of biomass burning emissions, lightning and convection on tropospheric CO, O_3 and H_2O levels over Indonesia and its surroundings during late 2006.

2. Description of Observations and Model Runs

2.1 TES Measurements

TES is a Fourier transform spectrometer that measures infrared emission of Earth's atmosphere with a focus on the troposphere. TES is on the Aura satellite, which has a ~705 km sun-synchronous near-polar orbit with an equator crossing time of ~13:45 and a 16-day repeat cycle.

The primary measurement mode for TES is the Global Survey (GS), during which it makes nadir observations with a 5.3 x 8.3 km^2 footprint, surveying the earth in 16 orbits (~26 hours). Measurements from subsequent TES orbit tracks in a GS are offset by 22º longitude such that near global coverage is obtained after one repeat cycle of 8 GS or approximately 16 days.

TES retrievals are based on the optimal estimation approach [*Rodgers*, 2000] and are described in *Worden et al.* [2004] and *Bowman et al.* [2002; 2006], with error characterization described in *Kulawik et al.* [2006]. Temperature, water vapor and O_3 are simultaneously retrieved in the first step of the retrieval with other species and parameters retrieved in subsequent steps. In version 2 (v02 or F03_03), TES retrieved profiles are provided on a 67-level vertical grid from the surface to 0.1 hPa.

Validation of TES V002 O_3 retrievals using ~1600 coincidences with ozonesondes by *Nassar et al.* [2008] indicated a high bias of 3-10 ppb with variation related to latitude zone and season. Similar results were found by *Richards et al.* [2008] using aircraft lidar measurements. Comparisons of TES V002 CO and Measurement of Pollution in the Troposphere (MOPITT) CO indicated consistency between the datasets [*Luo et al.*, 2007a], while comparisons of TES CO with in situ aircraft measurements showed agreement within ±15% [*Luo et al.* 2007b; *Lopez et al.*, 2008]. TES V003 H_2O vapor profiles were found to be ~5% high in the lower troposphere and up to ~15% high in the upper troposphere relative to Vaisala radiosonde measurements [*Shephard et al.* 2008]. This is believed to be slightly better than V002 H_2O used in the present work.

In cloud-free conditions, TES nadir O_3 profiles typically have nearly two degrees of freedom for signal (DOFS) in the tropical troposphere [*Bowman et al.*, 2002; 2006; *Worden et al.*, 2004; *Worden et al.*, 2007], and thus can be thought of as containing independent information on upper tropospheric and lower tropospheric O_3. The strength of the TES CO signal has varied over time, primarily as a result of instrument sensitivity. From 29 November 2005 to 2 December 2005, the TES optical bench was warmed to remove the build-up of contaminants on instrument optics. This procedure improves the measured signal, primarily impacting the spectral frequencies of the CO retrievals. Prior to decontamination, CO typically had 0.7-0.8 DOFS but following the procedure, CO has 1.4-1.5 DOFS in the troposphere [*Rinsland et al.*, 2006]. TES water vapor profiles typically have 3-5 DOFS (or a vertical resolution of ~3.5 km), nearly all of which correspond to the troposphere since air above the tropopause is comparatively dry [*Shephard et al.*, 2008].

All TES O_3, CO and H_2O data used in this work were screened to remove cloudy profiles (defined as having an effective optical depth greater than 2.0 and cloud top height above 750 hPa) and other potentially erroneous profiles using the recommended TES data quality flags. Ozone underwent additional screening based on the emission layer flag [*Nassar et al.*, 2008]. Upper tropospheric H_2O had additional filtering applied to prevent erroneous extreme high outliers from skewing the average VMR, by rejecting points with a VMR greater than 10 parts per thousand (ppth) above 510 hPa.

The optimal estimation approach used in TES retrievals combines information from a measurement with a priori knowledge of a given quantity to produce an estimate with greater

precision than either the measurement or a priori has independently. However, the accuracy of this estimate only improves if the a priori used does not introduce a bias. TES O_3 and CO a priori distributions vary by month (both vertically and horizontally) and come from averaged MOZART model runs [*Brasseur et al.*, 1998], while TES V002 monthly H_2O a priori distributions come from averaged GEOS-4 analyses. To avoid introducing biases, we apply uniform a priori profiles (calculated by averaging the July prior for a given species for 30ºS-30ºN) to all TES O_3, CO and H_2O data so that any spatial variation comes exclusively from the measurements. A uniform a priori has been applied to TES data in several other studies [i.e. *Zhang et al.*, 2006; *Luo et al.*, 2007a; *Logan et al.*, 2008] with the procedure and implications discussed in *Kulawik et al.* [2008].

2.2 GEOS-Chem

Model simulations were carried out using the chemical transport model GEOS-Chem [*Bey et al.*, 2001], which uses assimilated meteorology from the Goddard Earth Observing System version 4 (GEOS-4). Unless otherwise stated, model runs were based on a modified model version 7-04-10, in which the method used to constrain the lightning spatial distribution was improved as described below. This modification has since been incorporated into the standard GEOS-Chem code as of v7-04-12. Updated descriptions of the O_3-NO_x-hydrocarbon-aerosol simulation can be found in *Park et al.* [2006] and *Hudman et al.* [2007]. Modifications implemented to the standard biomass burning module are also described below.

The simulations used the EDGAR fossil fuel inventories for CO, NO_x and SO_2 for the year 2000 [*Olivier and Berdowski*, 2001] (scaled forward to 2002), implemented in GEOS-Chem by *van Donkelaar et al.* [2008]. These were overwritten with the following regional inventories: the Co-operative Programme for Monitoring and Evaluation of the Long-range Transmission of Air Pollutants in Europe (EMEP) inventory for Europe in 2000 [*Vestreng and Klein*, 2002], the Environmental Protection Agency's National Emission Inventory 1999 (EPA-NEI-99) for the U.S., the Big Bend Regional Aerosol and Visibility Observational (BRAVO) Study Emissions Inventory for Mexico in 1999 [*Kuhns et al.*, 2003], and the inventories of *Streets et al.* [2003] for Asia in 2000 and of *Streets et al.* [2006] for CO from China in 2001. Anthropogenic hydrocarbon emissions are described in *Bey et al.* [2001] and were scaled forward to 1998.

Biogenic emissions are based on the Model of Emissions of Gases and Aerosols from Nature (MEGAN) [*Guenther et al.*, 2006] which computes emissions for plant functional types as a function of temperature, solar radiation, leaf area index and leaf age. Biofuel emissions are from the generic annual inventory of *Yevich and Logan* [2003]. Biomass burning emissions are from the Global Fire Emission Database version 2 (GFEDv2 or simply GFED below) [*van der Werf et al.*, 2006] which uses Moderate Resolution Imaging Spectroradiometer (MODIS) fire counts [*Giglio et al.*, 2006] to determine the locations and times of active biomass burning areas. Emission of CO and other combustion by-products in GFED are calculated based on emission factors for each species and for three vegetation types (savanna, tropical forest and temperate forest). For this work we implemented the 8-day GFED emissions in GEOS-Chem. These were derived by resampling the inventory to 8 day means using MODIS fire hot spots [*Giglio et al.*, 2003; www.ess.uci.edu/~jranders/].

In earlier versions of GEOS-Chem, the spatial distribution of NO_x emissions from lightning was determined directly from cloud top heights (CTHs) in the GEOS meteorological fields. The parameterization based on *Price and Rind* [1992] calculated flash densities as a power-function of convective CTHs with vertical profiles of NO_x from *Pickering et al.* [1998], as implemented in *Wang et al.* [1998]. Knowledge of the global lightning distribution has since been greatly improved by the combined climatological product of the Optical Transient Detector (OTD) on the Micro-Lab 1 satellite, which measured lightning flashes from a near-polar orbit with a 70º inclination from April 1995 to March 2000 [*Christian et al.*, 1996; 2003; *Mach et al.*, 2007], and from the Lightning Imaging Sensor (LIS) [*Christian et al.*, 1992; *Mach et al.*, 2007] on the Tropical Rainfall Measuring Mission (TRMM) satellite which has been making lightning flash observations since December 1997 from ~35ºN to ~35ºS.

The cloud top height scheme gives the overall best simulation of the global lightning distribution within the GEOS-4 meteorological framework, relative to others in the literature. However, it fails to capture relative magnitudes between the predominant large-scale lightning features, and its separate equations for marine and continental boxes do not simulate well the local lightning patterns over the Maritime Continent. Various techniques have been used to constrain the GEOS-Chem distribution of lightning to match the satellite observations. *Stajner et al.* [2008] and *Jourdain et al.* [2008] adopted a regional approach, while *Sauvage et al.* [2007a] matched the model lightning at the grid-box level. In our approach, the model spatial distribution of lightning averaged over 11 years is constrained to match the 11-year High Resolution Monthly Climatology (HRMC v2.2) combined product of LIS/OTD (available from NASA's Global Hydrology and Climate Center GHCC), performed via monthly scaling factors applied at the model grid resolution. This approach is similar to the method of *Sauvage et al.* [2007a], but they used an earlier LIS/OTD product with coarser spatial and temporal smoothing, and constrained only with seasonal scale factors. Lightning NO_x injection heights follow the vertical distribution functions of *Pickering et al.* [1998], scaled to cloud top height and approximately 6 Tg N a^{-1} are released globally. The lightning parameterization used here is described in detail in *Murray et al.* (manuscript in preparation).

Initialization of the model consisted of a 9-month spin-up beginning in December 2004, followed by multiple runs (outlined in Table 1) spanning the 15 month period from September 2005 to December 2006. Model runs were carried out at the GEOS-4 resolution of 2º latitude by 2.5º longitude and a 30-level (reduced) vertical grid from the surface to 0.01 hPa. Model time steps were set to 15 minutes for transport and convection, and 60 minutes for emissions and chemistry.

Although the pure O_3 tracer is available in GEOS-Chem, the O_x tracer is much more commonly used and is essentially the same as O_3 but includes a contribution from NO_2 (which is only significant near the surface, close to strong sources) and a contribution from O which is only significant above the tropopause. Our focus below is on the 825-287 hPa range, which makes the O_x or O_3 distinction negligible, so for the remainder of the paper, we only refer to O_3 even if O_x was used. Water vapor is provided as a GEOS-4 meteorological field in the form specific humidity (q) and this quantity is directly converted to H_2O VMR.

2.3 TES and Model Comparison Method

To compare TES and model CO, O_3, and H_2O, the model was sampled at the position and closest time of the TES measurements. The CO and O_3 model output had 3-hour resolution while the GEOS-4 H_2O consisted of 6-hour averages. All TES profiles for a given model gridbox (typically 1-2) that correspond to the closest time were averaged. To increase the information content from TES measurements for all 3 species, we averaged the six TES levels spanning 825-511 hPa for the lower troposphere (LT) and the six levels spanning 464-287 hPa for the upper troposphere (UT), approximately corresponding to the tropospheric O_3 DOFS. The model profiles were interpolated to the TES 67-level vertical grid, accounting for variations in surface pressure, then transformed using the TES averaging kernel (AK) and a priori profiles to match the TES vertical resolution. The uniform TES a priori profiles mentioned in the previous section were also applied to the model results in all comparisons.

3. Results and Analysis

3.1 CO, O_3 and H_2O Distributions in Late 2006

Figure 1 shows maps of CO, O_3 and H_2O for October, November and December 2006 for the LT the TES observations (left), the model *Base* run with the corresponding TES averaging kernels applied, (herein referred to as GEOS-Chem wAK, center) and the difference (model wAK – TES, right). In the LT, there is ~1 DOFS for O_3, <1 for CO and ~2 for H_2O. In Figure 1 and many other figures, white pixels indicate an absence of TES observations in those grid boxes. TES data plotted here are the same as in *Logan et al.* [2008], but here we show a higher horizontal resolution and average six TES vertical levels rather than using a single level, 511 hPa.

The TES CO maps show a very strong maximum over Indonesia and the Indian Ocean, which exceeds 200 ppb in October and November, but essentially disappears in December. Secondary maxima are also observed over South America, Africa and China. CO spatial distributions from TES and the model in Figure 1 agree very well in terms of the shapes and locations of these prominent CO maxima, but model CO is systematically lower than TES. The difference map shows that this bias is typically less than one division on the color scale (10 ppb). The model is too low by more than 30 ppb in the regions of Indonesia (particularly November), eastern China (October only) and southwestern Africa, while the model is slightly high over western South America. These differences exceed the TES bias of ±10 ppb (*Luo et al.*, 2007; *Lopez et al.*, 2008]. Overall, there is very little difference between TES CO in the LT and UT (not shown) due to the limited DOFS available from TES. In October, separate Indonesian-Indian Ocean and eastern China CO maxima are resolved, unlike in *Logan et al.* [2008], resulting from the inclusion of information from lower levels. Very high CO levels in this region were also observed by the Atmospheric Chemistry Experiment Fourier Transform Spectrometer (ACE-FTS) [*Rinsland et al.*, 2008] and the Measurement of Pollution in the Troposphere (MOPITT) instrument (*http://web.eos.ucar.edu/mopitt/*) around the same time.

Figure 1 shows some similarities between TES and GEOS-Chem O_3, for example, both show a minimum in O_3 over the tropical Pacific Ocean and to a lesser extent over the equatorial Indian Ocean. The highest TES O_3 levels are found in the southern tropics extending west from the east coast of South America to the northwest coast of Australia and the southern coast of the Indonesian island of Java. GEOS-Chem O_3 generally agrees well with the spatial patterns seen

by TES but is as much as 20-30 ppb lower than TES over portions of the tropical Atlantic and western Africa in October. The model O_3 is also too low by 10-25 ppb over parts of the eastern Indian Ocean in November and December. These differences exceed the 1σ high bias of 3-10 ppb identified during TES V002 O_3 validation [*Nassar et al.*, 2008]. The TES and GEOS-Chem distributions have numerous similarities to the tropospheric O_3 residual distributions determined from a combination of Ozone Monitoring Instrument (OMI) and Microwave Limb Sounder (MLS) for the same time period [*Chandra et al.*, 2009]. Figure 2 compares model profiles to soundings at Java, Kuala Lumpur and Samoa from the Southern Hemisphere Additional Ozonesonde (SHADOZ) network [*Thompson et al.*, 2003: 2007] in late 2005 and 2006, indicating excellent overall agreement, with the largest discrepancies in November 2006.

Figure 1 shows excellent agreement between TES and GEOS-4 H_2O, considering the large variability in tropospheric H_2O. No obvious bias is revealed, only single scattered grid boxes are too high or low.

3.2 2006-2005 CO, O_3 and H_2O Anomalies

Figure 3 shows the difference between 2006 and 2005 for the LT in October, November and December for TES (left) and the GEOS-Chem *Base* run wAK (right); results for the UT are similar, so are not shown. These differences, which we will refer to as anomalies, remove some systematic errors such as retrievals biases or any remaining effect of a priori values (although this has primarily been dealt with by application of a constant prior to TES and the model), and model biases. Figure 3 shows a very strong positive CO anomaly from TES in the vicinity of Indonesia in October and November 2006, which is essentially absent in December. A much weaker negative anomaly is seen over the equatorial eastern Pacific, South America and the south Atlantic in October that is reduced in November, then shifts to western-equatorial Africa in December. The positive CO anomaly closely resembles the large CO maximum in Figure 1, but agreement between TES and the *Base* model anomalies is better, most likely because some biases cancel.

Figure 3 shows a strong positive O_3 anomaly of as much as ~30 ppb over Indonesia and the eastern Indian Ocean including the Bay of Bengal, which is not evident from Figure 1 since O_3 is low in this region. The area of elevated O_3 is largest in October 2006 and decreases in extent in November and December in both the TES measurements and the model. The model matches the observed anomaly well in October, except in the Bay of Bengal, but underestimates it in November and December. One notable deficiency in the model is the division of the major positive anomaly in December due to a weakening of the anomaly over Indonesia (at 10ºS-10ºN), which is not seen in the observations. The negative lobe of the El Nino 'asymmetric dipole anomaly' for O_3 as described by *Chandra et al.* [1998; 2007], is observed over the central Pacific in October and December, but is noticeably absent in November for both TES and the model. The dipole anomaly is also evident in the sonde data and model comparisons in Figure 2. Ozone is lower at Java and Kuala Lumpur in October-December 2005 than in 2006, while it is higher in those months at Samoa in 2005 than in 2006, and the model captures most of these differences. Both TES and the model also show another negative O_3 anomaly over equatorial Africa which is strongest in December; this anomaly may be the IOD analogue to the El Niño Pacific O_3 anomaly.

TES and GEOS-4 H_2O anomalies show excellent agreement. Interestingly, the 10ºS-10ºN gap in the December positive O_3 anomaly in Figure 3 coincides with a similar gap in the negative H_2O anomalies from both TES and GEOS-4. An inverse relationship can be seen between many of the H_2O anomalies and co-located O_3 anomalies of the opposite sign, but upon close inspection, the largest positive O_3 anomaly in October is not entirely co-located with the strong negative H_2O anomaly which is smaller in extent and peaks more to the south. Reasons for similarities and differences between the CO, O_3 and H_2O anomalies and between TES and GEOS-Chem are explored below.

3.3 The Influence of Biomass Burning Emissions

Logan et al. [2008] showed CO anomalies similar to those in Figure 3 and attributed the large Indonesia and equatorial Indian Ocean anomaly during October and November to severe biomass burning in Indonesia during the 2006 drought. We ran the model for 2006 using GFED emissions for the corresponding months in 2005 (designated '*2006e05*') to quantify the effect of changes in biomass burning emissions on CO and O_3. As expected, the large CO anomaly around Indonesia in October and November essentially disappears (Figure 4) since GFED emissions of CO from Indonesia were only 5.8 Tg in September to December 2005 compared with 67.3 Tg for the same period in 2006.

Large anomalies for O_3 remain from the *2006e05* simulation. It is striking that the component of the O_3 anomaly unrelated to biomass burning is coincident with the observed H_2O anomaly, while the component of the O_3 anomaly near Indonesia in Figure 3 that is related to biomass burning is essentially coincident with that for CO (10ºN-10º), particularly in October. These results for 2006 confirm earlier findings denoting contributions to elevated O_3 from both biomass burning and meteorology during the 1997 El Niño event [*Hauglustaine et al.*, 1999; *Sudo and Takahashi*, 2001; *Thompson et al.*, 2001; *Chandra et al.*, 2002; *Duncan et al.*, 2003a]. However, our model analysis in combination with TES data allows better delineation of the location of these effects.

Comparisons of CO simulated using 8-day and monthly GFED emissions (not shown) show little difference for averages of a month or longer, but a significant difference is found when working with half-month or shorter timescales. To better understand the time evolution of the CO and O_3 enhancements, we take advantage of the 16-day repeat cycle of TES global surveys and the GFED 8-day resolution. Figure 5 shows CO for half-month intervals from TES and GEOS-Chem, with the exact time periods given in Table 2, selected to avoid splitting TES global surveys.

Figure 5 illustrates the dramatic change in the CO maximum in the Indian Ocean between the first and second half of November in both the observations and the model. The time evolution of CO, O_3, and H_2O averaged over the box region (11ºS-5ºN and 91.25-121.25ºE) corresponding to peak CO is shown in Figure 6. Averages for the LT and UT are given for O_3 and H_2O, but only for the LT for CO as the UT average is very similar. These plots reinforce that the model is systematically low relative to TES for both CO and O_3. TES O_3 has a well-established systematic high bias as noted above. Validation showed that TES O_3 was high by ~3 ppb in the

UT and ~9 ppb in the LT in the tropics (15ºN-15ºS) [*Nassar et al.*, 2008], so these quantities were subtracted from the TES time-series as a bias correction (Figure 6), reducing the difference between the base model simulation and TES O_3. We opted not to apply a bias correction to the O_3 maps since they span 30ºS-30ºN, and validation work identified different values of the bias for the tropics, northern subtropics and southern subtropics [*Nassar et al.*, 2008]. No correction is applied for either TES CO or H_2O, as these biases are not as well-characterized.

A sharp decrease in model CO is apparent in the first half of November, prior to a decrease in TES CO. GFED CO biomass burning emissions for the same region are also shown in Figure 6 as half-month averages. Since the time evolution of model CO closely follows that of the GFED emissions, we evaluate the timing in GFED by comparing with precipitation data. Precipitation data (http://www.tutiempo.net/) is shown in Figure 7 for two sites in southern Borneo near the 2006 fires, Palangkaraya (1ºS, 114ºE) and Banjarmasin (3.43ºS, 114.75ºE). Clearly, the high GFED emissions correspond to the long dry period. The 1.02 mm of rain recorded at Palangkaraya on October 22 is the only evidence for a reduction in biomass burning emissions for the October 16-23 period. The onset of rain at Banjarmasin on November 3 and Palangkaraya on November 6 correspond with the reduction of CO emissions in early November. Whether or not these small quantities of rain could have such a large effect on CO emissions from the fires is not clear. In 1997, the vast majority of fire emissions from Borneo were the result of peat burning [*Levine* 1999], which tends to smolder after the onset of rain [*Khandekar et al.*, 2000], and this is likely the case also in 2006. Since GFED determines emissions based on MODIS fire counts, it only includes actively flaming fires and does not directly account for fires that are dying out and smoldering, although these likely emit CO with a higher CO/CO_2 ratio for the same fuel load due to more incomplete combustion. To account for continuing CO emissions after the onset of rain as a result of smoldering peat, we ran the model with various scaling factors applied to GFED emissions for November, followed by a return to normal emissions in December. A scaling factor of 3 best reproduced the shape of the LT and UT CO timeseries lines (Figure 6) and made a modest improvement to the shape of the O_3 timeseries.

The time evolution of O_3 differs between TES and the model in a more complicated way than for CO, suggesting contributions from multiple factors. The model O_3 matches the time evolution from TES within a few ppb from early September to early November in the run with increased November emissions. However, the model O_3 decreases by ~ 9 ppb from early to late November in the LT (~ 7 ppb in the UT), while TES O_3 increases slightly in the LT, and stays constant in the UT. Model and observed O_3 decrease thereafter, at about the same rate, but the model is systematically low by ~ 5 ppb in the LT and ~8 ppb in the UT.

We estimate the contribution from Indonesian biomass burning to the O_3 anomaly using the model run with increased GFED emissions in November, again comparing to the run with 2005 GFED emissions (*2006e05*). Figure 8 shows the total 2006-2005 O_3 anomalies in each month (with the TES AK applied), the contribution resulting from enhanced burning in 2006, and the contribution from other factors. Figure 8 indicates that the O_3 anomaly caused only by enhanced biomass burning in 2006 (relative to 2005) is located primarily from the equator to 10ºS and west of 120ºE in October, while that caused by factors related to dynamics is located primarily at 10º-20ºS and extends east as well as west of 120ºE. There is also a disconnect between the locations

of the biomass burning related anomaly and the main dynamically related anomaly in November. The spatial extent of the dynamically related anomalies is larger.

Even in the equatorial region however, there is an influence of factors other than biomass burning on O_3. This is quantified for the box region by comparing the results for the *2006e05* run (dashed blue line in Figure 6), the run with increased GFED emissions in November in 2006, and the 2005 Base run. For this box we find that the fires in 2006 accounted for an average of ~45% of the O_3 anomaly in October, ~75% in early November, ~45% in late November, and only 10% in December (Table 3).

3.4 Lightning and its Contribution to O_3

Logan et al. [2008] hypothesized that the persistence of the O_3 anomaly weeks after the large CO anomaly had disappeared could be related to enhanced lightning NO_x emissions over Indonesia and New Guinea, since LIS flash rates in November and December 2006 were as much as 200% higher than those in 2005 at certain locations on these islands. A comparison of the lightning flash rates between GEOS-Chem and LIS observations (Figure 9) indicates that the model significantly underestimates the differences over Indonesia and New Guinea in November and December of the two years. *Hamid et al.* [2001] showed that during the 1997 El Niño (which also had a positive IOD), convection over Indonesia was less frequent but more intense than usual and that there was a significant overall increase in regional lightning activity. Figure 9 demonstrates that the lightning parameterization used here, based on cloud top height in the GEOS-4 convection scheme and on mean spatial patterns from LIS data, does not capture the correct interannual variability of lightning. In particular it does not capture the difference between a neutral ENSO year and one with a coincident El Niño and positive IOD.

To quantify the effects of lightning NO_x on tropospheric O_3 in 2005 and 2006, we ran the model with these NO_x emissions turned off (*NoLight*) and the compared results to a baseline run from the same model version (v7-04-13). Differences (with the TES AK and constant a priori applied) are shown for October to December of each year in Figure 10. Lightning NO_x increases O_3 throughout the tropics with sensitivities peaking in the tropical south Atlantic at ~50-60 ppb in the UT and ~30-40 ppb in the LT. Near Indonesia and over the Indian Ocean, the sensitivity is much less, rarely exceeding 10 ppb.

Figure 10 also shows the O_3 anomaly for the *NoLight* runs. The monthly anomalies over Indonesia and the Indian Ocean are very similar to those in Figure 3 for the runs with NO_x from lightning, implying a modest contribution of lightning to the anomaly. However, there is a much smaller negative O_3 anomaly over equatorial Africa in December in the *NoLight* runs compared to Figure 3, showing a much larger impact of differences in lightning NO_x between the two years there.

Duncan et al. [2003a] used GEOS-Chem with an older lightning parameterization to conduct a similar sensitivity test for the 1997 El Niño, turning off lighting for September-December. They found that the global lightning contribution to daily O_3 profiles over Java reached a maximum of 15-25 ppb between 400 and 200 hPa UT, and was much less at lower altitudes. *Sauvage et al.* [2007b] ran GEOS-Chem, separately applying a 1% decrease to NO_x emissions from lightning,

soils, biomass burning and fossil fuel emissions over all seasons, indicating that O_3 was more sensitive to the change in lightning NO_x than to changes in other NO_x sources, but they did not evaluate the effects of perturbing emissions of other O_3 precursors such as CO that also result from biomass burning. The spatial distributions of O_3 enhancements resulting from the lighting NO_x in Figure 10 and in *Sauvage et al.* [2007b] show similar features.

Since lightning in our baseline model runs produces up to 10 ppb O_3 over Indonesia and the Indian Ocean, the enhancement of lightning during the positive phase of ENSO and the IOD could account for a portion of the 2006-2005 anomaly and help to explain the TES-model discrepancy. We addressed this by scaling the model lightning from October to December 2006 according to flash rate ratios from the LIS Science Data product for 2006:2005. These scale factors, f_{mon}, calculated for land grid boxes in Indonesia and New Guinea (9ºN-13ºS and 93.75-151.25ºE) were 0.6 for October, 1.4 for November and 2.0 for December. Scaling lightning reduces O_3 in 2006 up to ~3 ppb in the LT and ~5 ppb in the UT in October, followed by slightly larger enhancements in November. In December, O_3 is enhanced by ~5 ppb in the LT and by ~10 ppb in the UT, with the enhancement centered at about 5ºS. When these localized changes are averaged over the box region for the time-series, they are reduced as shown in Figure 11. Scaling lightning produces better agreement with the corrected TES O_3 data for October, but differences remain in late November and early December.

Precipitation histograms (as in Figure 7) for multiple locations throughout Indonesia and New Guinea indicate much more precipitation in the second half November than in the first, which agrees with the decrease in CO observed during November (Figure 5), and with the increase in convection in late November that is discussed below (Section 3.6). Assuming that lightning is coincident with local precipitation, we re-calculate scale factors for October and November taking f_{mon} as $\frac{1}{2}(f_1+f_2)$ where f_1 and f_2 are factors for the first and second half of each month. Since October lightning is weak, rescaling its lightning is less important than November; however, we assume factors of f_1=1 and f_2=0.20 for October and f_1=1 and f_2=1.80 for November, which when averaged over the month, match the monthly factors. (December lightning was not re-scaled.)

Changes to O_3 as a result of modifying biomass burning emissions and lightning emissions are not necessarily additive, so we ran the model applying both the lightning scaling and the GFED increase. Results in Figure 11 show that this run correctly simulates the continual increase in O_3 during the first half of November in the LT, but still results in a discrepancy for the remainder of the month and early December. Comparisons between O_3 from this model run and sondes (Figure 2) also indicates improvements for the Kuala Lumpur and Java stations, but almost no change for Samoa.

3.5 Water Vapor

Chandra et al. [1998] and others have shown that during the 1997 El Niño, high O_3 coincided with low H_2O vapor (at 215 hPa) and weak convection. We demonstrated this inverse relationship between O_3 and H_2O anomalies in the LT in Figure 3. Water vapor increases the rate of O_3 destruction by producing $O(^1D)$ radicals to react with H_2O to form HO_x, but HO_x contributes to O_3 production when sufficient NO_x is present. Although these mechanisms work

in opposite directions, for low NO_x (~<0.10 ppb), O_3 destruction dominates, thus increased H_2O decreases O_3, while if NO_x is higher, O_3 production dominates, thus increased H_2O increases O_3 [*Klonecki and Levy*, 1997].

The time evolution of H_2O vapor in TES and the model is shown in Figure 6. After filtering the TES data to remove extreme outliers, there is very good agreement in the LT and UT for 2005 and 2006 (with the exception of late September 2005, which only had a single TES global survey, shown in Table 2), although there is a small systematic difference in the LT from October to December 2006, during which time GEOS-4 is higher than TES by ~5%. Validation of GEOS-4 humidity indicates that it is similar to that from the European Centre for Medium Range Weather Forecasting (ECMWF), but GEOS-4 had a UT moist bias over the ocean [*Bloom et al.*, 2005]. To determine if errors in GEOS-4 H_2O were impacting O_3, we carried out a simulation with H_2O reduced by 10% in the box region for November and December 2006. This produced a peak increase in O_3 of ~6%, but a mean increase of only 1-2%, suggesting that effects of H_2O vapor on production and destruction of O_3 nearly balance.

3.6 Dynamical Factors

Horizontal winds at 700 hPa for the region are shown for half-month intervals in October and November 2006 in Figure 12. Although the winds over Java and Borneo are generally westerly in 2005 (not shown), in 2006 they are westerly only in early October. There is easterly equatorial flow over Indonesia from late October to late November 2006. The effect of the change in wind flow in 2006 is also evident in Figure 5 where the high CO air mass is dispersed northeast toward the Pacific during the first half of October, then subsequently west toward the Indian Ocean. The dispersion of CO is consistent with the weak winds near the western Pacific and the Maritime continent. This pattern of weak transport is similar to that during the 1997 El Niño [*Duncan et al.*, 2003a]. In 2006, the flow from northern Australia in late November also serves transport biomass burning emissions towards the Indian Ocean.

Accurate representation of atmospheric convection in global models is difficult, in part because convective processes occur on sub-grid scales. GEOS-4 uses the Zhang and McFarlane (ZM) parameterization [*Zhang and McFarlane*, 1995] for deep convection with updraft mass flux, downdraft mass flux and updraft entrainment provided as 6-hour averages. Shallow convection is parameterized separately based on *Hack et al.* [1994].

We tested the effect of convection on CO and O_3 in the model by globally turning off all three ZM deep convection parameters in GEOS-4, while shallow convection was not changed. Figure 13 shows the difference between our *Base* run and runs with no convection (but identical water and lightning) for November 2006 at four model levels. Each half-month period began with the initial tracer concentrations from the *Base* run to isolate the contribution from convection for that time period. Convection generally reduces CO in the boundary layer (BL) and LT, but increases it in the UT up to the base of the tropical tropopause layer (TTL), near 14 km. If a strong surface CO source is present, as in the beginning of November over Indonesia and the Indian Ocean, convection lofts the CO up to the UT, largely reducing it in the LT, especially in the BL. In the absence of a strong CO source, as for late November and the remainder of the year (not shown), reductions in BL and LT CO are smaller and almost equal in magnitude.

The effect of convection on O_3 is nearly opposite that of CO, with convection generally increasing O_3 in the BL and LT, but decreasing it in the UT and base of the TTL. This can be understood by assuming that convection directly transports air from the LT (containing low levels of O_3) to the UT and the associated mixing transports O_3 rich air from the UT down to the LT where the O_3 lifetime is shorter; however, Figure 2 indicates that our O_3 profiles are nearly vertical throughout the troposphere. Furthermore, convection also transports O_3 precursors like CO and NO_x, which will reduce LT O_3 and increase UT O_3. These competing mechanisms, described in earlier work [*Lawrence et al.*, 2003; *Doherty et al.* 2005], indicate that convection undoubtedly impacts O_3, but the net effect depends on the balance between multiple factors. As noted by *Lawrence and Salzmann* [2008], such tests have significant limitations, because of the relationship between parameterized deep convection and the large scale circulation which is not treated correctly when convection is turned off in the model.

Observations tell a clearer story about the relationship between convection and O_3 in our region of interest. During El Niño, when there is weaker convection than normal over the maritime continent and eastern Indian Ocean, O_3 is higher in the LT and UT; conversely, over the central Pacific, where convection is stronger than normal, O_3 is lower during El Niño. Here we use OLR data as a surrogate for deep convective activity, and compare OLR to the time evolution of the updraft air mass flux in GEOS-4. Observed OLR is interpolated from satellite brightness temperature data by NOAA [*Liebmann and Smith*, 1996; www.cdc.noaa.gov/cdc/data.interp_OLR.html].

Figure 11 shows GEOS-4 updraft air mass fluxes for model levels at ~6.6 km and ~10.0 km (multiplied by a factor of 4) for the box region used in the time series plots. The mass flux increases steadily from early October to year end, qualitatively consistent with H_2O increases in TES and GEOS-Chem (Figure 6). The OLR data are plotted with the vertical axis reversed, since low values of OLR indicate high clouds and hence convection. The GEOS-4 OLR line resembles the updraft mass flux, with a decrease beginning in early October and continuing to the end of 2006, consistent with strengthening convection. NOAA OLR is systematically lower than GEOS-4 OLR, but more importantly it hardly changes in October, then decreases steadily from November to year end. Assuming some consistency between GEOS-4 convection and OLR implies that GEOS-4 convection starts to increase about a month too early.

Figure 14 shows anomaly maps of GEOS-4 and NOAA OLR at half-month intervals, indicating many similarities between the OLR data sets. Increased OLR (decreased convection) is found over most of the Indonesia and New Guinea region in late 2006, with a larger and more contiguous positive anomaly in the NOAA OLR than in the GEOS-4 OLR. This implies that the reduction in convection in late 2006 during El Niño was not large enough in the model. There are even small areas north of the equator in late October and early November where OLR is lower in 2006 than in 2005 in the model (implying increased convection in 2006), but not in the NOAA OLR. A direct comparison of GEOS-4 and NOAA OLR in 2006 (Figure 15) also implies that there is too strong convection in the model north of the equator from late October until late November, except over land. (GEOS-4 OLR was reduced by 13 W/m^2 based on the mean offset from NOAA OLR in Figure 11.) The OLR data imply that GEOS-4 convection is too weak over

Java, Borneo and New Guinea, which is consistent with the underestimate of lightning in this region.

Too vigorous convection in GEOS-4 during November and December, the months with most active convection in 2006, is likely responsible for the underestimate of O_3 (Figures 1 and 11), and for the underestimate of the O_3 anomaly (Figure 3). The underestimate of the anomaly is most obvious north of the equator, the area with the largest mismatch between model and NOAA OLR, but there is also an underestimate south of the equator. Overly vigorous convection in a normal year, when the convection is very active anyway, appears to be less of a problem for model O_3, since the model reproduces observed O_3 profiles in 2005, as shown by the sonde data comparisons in Figure 2 and by TES comparisons in Figure 6.

Both the GEOS-4 and NOAA OLR show decreased OLR (increased convection) over the central Pacific. Increased convection here is responsible for the co-located reduction in O_3 during El Niño [*Chandra et al.*, 1998]. We noted earlier that both the TES data and the model show a negative O_3 anomaly in October (east of the date-line), but that it disappears in November, and returns weakly in December. The OLR data show only a weak convection anomaly east of the date-line in early October. It weakens for a month, then strengthens until the end of the year.

The most prominent negative OLR anomaly is over the western Indian Ocean and east equatorial Africa in late November and December. The increase in convection in 2006 contributed to the prominent negative anomaly in O_3 in December in eastern Africa seen in the TES data and the model (Figure 3).

3.7 Soil NO_x Emissions

Another factor contributing to O_3 that may not be well-represented in the model is the release of NO_x from soil, which occurs both gradually and as a pulse at the onset of heavy rains. Recent estimates of soil NO_x emissions suggest a global source of 8.9 TgN/yr [*Jaeglé et al.*, 2005], which is much larger than most earlier estimates. In northern Africa, which accounts for 30% of global soil NO_x, pulses have been shown to last for 1-3 weeks after the onset of rain [*Jaeglé et al.*, 2004].

GEOS-Chem accounts for soil NO_x emissions based on the approach of *Yienger and Levy* [1995], in which a very low, baseline level of emissions are constantly released from wet soil, but at the onset of rain, this background is multiplied by a scale factor to simulate a pulse of NO_x emissions, which then decreases exponentially with time. The pulse strength depends on the rainfall rate with factors of 5 (relative to baseline emissions) for a sprinkle (1-5 mm/day), 10 for a shower (5-15 mm/day) and 15 for heavy rain (>15 mm/day). *Yienger and Levy* [1995] state that the range of likely scale factors spans 10-100. To investigate the effect of a hypothetical large NO_x pulse, we ran the model for November with a factor of 10 increase in soil NO_x coming from land within the same box used to scale lightning (Figure 9). This increase is minimal in the absence of precipitation, but increases the model scale factors to 50, 100, and 150 for a sprinkle, a shower, and heavy rain, respectively. Figure 16 shows the difference in O_3 between this run (*SoilNOx10*) and the *Base* run. Ozone increases first occur over land with the largest intensity

originating from the island of Sulawesi (east of Borneo), but transport carries O_3 and its precursors eastward, such that in the second half of November, the increase over Java and Borneo is on the order of 10 ppb in the LT and UT. Evidently, a larger increase in soil NO_x emissions after rainfall would remove some of the discrepancy in Figure 11 in late November and would improve the spatial pattern of the model anomaly in Figure 3 in November (and likely December) in the equatorial region.

4. Discussion and Conclusions

A moderate El Niño and the positive phase of the IOD were coincident in late 2006 for the first time since 1997 and only the fourth time in ~50 years. From mid-September to mid-November, Indonesia experienced severe ENSO-IOD-induced drought permitting intense biomass burning in southern Borneo [*Field and Shen*, 2008]. This burning decreased abruptly in mid-November as heavy rains began. TES, which provides simultaneous, coincident, nadir measurements of CO, O_3 and H_2O from space, observed elevated O_3 and CO above Indonesia and the eastern Indian Ocean during late 2006 [*Logan et al*., 2008]. Carbon monoxide exceeded 200 ppb in the LT in the area of peak intensity throughout October and early November. Ozone observations exceeded values from 2005 (a neutral ENSO year) by 12-18 ppb in the LT and 15-24 ppb in the UT from October to mid-December, but the O_3 anomaly was not entirely coincident in space and time with the elevated CO.

GEOS-Chem model simulations exhibit the main features in tropospheric CO and O_3 that were observed by TES during late 2006, indicating that most important chemical and physical processes are understood and are accounted for by the model. This study is the first to use simultaneous measurements of tropospheric CO, O_3 and H_2O to evaluate model results. The CO data enabled us to test the GFED bottom-up estimates of CO emissions from the massive Indonesian fires in 2006. We confirm previous findings which suggest that elevated O_3 during an El Niño results from a combination of biomass burning and dynamical factors [*Hauglustaine et al.*, 1999; *Sudo and Takahasi*, 2001; *Thompson et al.*, 2001; *Chandra et al.*, 2002], but we investigate the causes of O_3 changes in greater detail. By examining CO and O_3 changes at higher spatio-temporal resolution than in earlier studies, and by investigating the roles of biomass burning, lightning, winds, convection, H_2O, and soil NO_x, we uncover some limitations in the model and in our understanding of the detailed mechanisms for elevated O_3 and CO.

The decrease in CO in the LT in late November and December occurs more rapidly in the model than in TES observations, even with the use of 8-day GFED biomass burning emissions. This likely occurs because the GFED inventory is based on MODIS fire counts, which do not account for CO emissions from smoldering stage of fires, which are significant for peat fires in Borneo. It was necessary to increase GFED emissions for Indonesia by a factor of 3 in November 2006 to obtain consistency with the time evolution of the TES CO observations.

It proved more difficult to reproduce the temporal and spatial evolution of the O_3 anomaly in late 2006; the model does best in October. The adjusted GFED emissions in November improve the model simulation of O_3 in early November, but the model starts to decrease two week too early, in late November, and thereafter is lower than TES observations. We explored if this could be

caused by the higher lightning NO_x emissions in 2006, as proposed in our earlier work [*Logan et al.*, 2008].

The LIS data show that lightning flash rates were as much as 200% higher in November and December 2006 than in 2005, but lower in October. Model lightning is derived from cloud top heights which seem to be underestimated over Indonesia and the neighboring islands in late 2006 (based on the OLR analysis), leading to underestimates in lightning NO_x. By adjusting the model lightning in 2006 based on LIS observations and the timing of precipitation, differences in lightning NO_x between 2005 and 2006 are shown to make a modest contribution (a few ppb) to the model O_3 anomaly. Sensitivity runs with no NO_x from lightning show that this source of NO_x contributes about 5-15 ppb O_3 in total in the equatorial band around Indonesia, with the largest contribution in the UT. The model run with adjusted lighting and adjusted GFED emissions matches the temporal evolution of LT O_3 very well in the equatorial box with highest CO until late November, when model O_3 starts to decrease two weeks early. In the UT, the model matches the temporal evolution of O_3 fairly well, but is too low by ~10 ppb from late October onwards.

Convective transport remains one of the most challenging processes for global models to represent accurately, yet convection changes during El Niño are very important contributors to the O_3 anomalies. Comparison of model OLR with that derived from observations implies that the convection is too strong in the model in 2006 in the Indonesian region, except over land where the model cloud top heights are too low (consistent with the lightning problem). Maps of NOAA OLR show that convection is most active near the Equator, where the O_3 anomaly is missing in December. Overly vigorous convection in the model appears to be the cause of the disparity between the observed and modeled O_3 anomaly in the eastern Indian Ocean and Indonesia from mid-November onwards, when convection starts to increase. Soil NO_x emissions after the onset of rain could also play a role in the disparity.

The asymmetric dipole anomaly relationship between O_3, H_2O, and convection observed during past El Niño events [*Chandra et al.*, 1998] is evident in 2006, with an inverse relationship for most of the H_2O and O_3 anomalies in both TES observations and the model (Figure 3). The Indonesian node of the dipole was strongest in October and decreased in November and December. The dipole node over the central Pacific (negative for O_3 and positive for H_2O) was present in October, temporarily weakened in November, and reappeared in December in both the model and observations.

The contribution of biomass burning emissions to the O_3 anomaly in the LT is generally less than 10 ppb, reaching more than 15 ppb only in October immediately downwind of the fires in Borneo. It is primarily located from the equator to 10ºS in October, but extends further south in November. By contrast, the anomaly related to dynamical factors is largest south of 10ºS, and is more extensive. It may be that the effect of the fire related anomaly in underestimated in the model because of the overly vigorous convection that starts too early in the model. In the region with highest CO, biomass burning emissions contribute ~45% of the O_3 anomaly in October and late November, ~75% in early November, and only 10% in December (Table 3).

The potential contribution to O_3 from emissions of NO_x from soil was investigated, since these emissions increase with the onset of rain [*Jaeglé et al.*, 2004; 2005]. The magnitude of increase is related to the strength of rain, with an uncertainty of at least an order of magnitude [*Yienger and Levy*, 1995]. Increasing soil NO_x emissions by a factor of 10 showed significant increases in O_3 in late November, suggesting this could be a contributing factor to the low O_3 in the model, particularly the underestimate in the equatorial band in November and December. This should be investigated in future work making use of available satellite measurements of NO_2 as a constraint.

Both the TES data and the model show a large negative O_3 anomaly (10-20 ppb) in equatorial Africa and the western Indian Ocean in December that is collocated with a positive H_2O anomaly and a positive convection anomaly (Figures 3 and 14). This feature starts to develop in November. The short rain season in eastern equatorial Africa is in October to December, and there was a drought in this region in late 2005 and heavy rainfall and severe flooding in late 2006 [*Shein et al.*, 2006; *Arguez, et al.*, 2007]. It is likely that this event was related more to the dynamics of the Indian Ocean basin rather than simply a response to El Nino, based on analyses of previous extreme rainfall events in this region [*Webster et al.*, 1999; *Saji et al.*, 1999]. The vigorous convection in late 2006 evidently caused the large decrease in O_3 relative to conditions in 2005. The O_3 anomaly extends further west than the H_2O anomaly in this region of easterlies, in the TES data and in the model.

There has been considerable analysis of the effects of the 1997 El Niño [for example *Chandra et al.*, 1998; *Hauglustaine et al.*, 2001; *Sudo and Takahashi*, 2001; *Thompson et al.*, 2001; *Duncan et al.*, 2003a], because of the important role that ENSO plays in tropical atmospheric chemistry as discussed in the Introduction. The present work provides a more detailed analysis of the effects of the 2006 El Niño than was possible for the 1997 event, because of the availability of satellite observations of CO, O_3, H_2O, fires, and lightning. While not as strong as the El Niño in 1997, the 2006 event shared similarities such as the IOD influence. The coincident IOD appears to reinforce some El Niño effects for the region such that the combination produces an impact similar to a stronger El Niño than the Pacific SST anomalies would suggest, including the severe drought and very intense biomass burning in Borneo. ENSO is the dominant mode of tropical tropospheric variability and contemporary El Niño conditions in the tropics may provide a preview of future anthropogenically-induced climate warming, thus it is important to use observed changes in atmospheric composition induced by these events to challenge and improve global models.

Acknowledgments

This work was funded by National Aeronautics and Space Administration (NASA) grants to Harvard University including grant NNX071B17G.

References

Aldhous, P. (2004), Borneo is burning, *Nature*, 432,144-146.

Arguez, A., A. M. Waple, A. M. Sanchez-Lugo (2007), State of the climate, 2006, *Bull. Am. Met. Soc., 8*, S8-S135.

Bacastow, R. B. (1976), Modulation of atmospheric carbon dioxide by the Southern Oscillation, *Nature*, 261, 116-118.

Beer, R., T.A. Glavich, D.M. Rider (2001), Tropospheric Emission Spectrometer for the Earth Observing System's Aura satellite, *Appl. Opt.*, 40, 2356–2367.

Beer, R. (2006), TES on the Aura Mission: Scientific Objectives, Measurements, and Analysis Overview, *IEEE Trans. Geosci. Remote Sens.*, 44(5), 1102-1105.

Bey, I., D. J. Jacob, R. M. Yantosca, J. A. Logan, B. D. Field, A. M. Fiore, Q. Li, H. Liu, L. J. Mickley, and M. G. Schultz (2001), Global modeling of tropospheric chemistry with assimilated meteorology: Model description and evaluation, *J. Geophys. Res.*, 106, 23,073– 23,089.

Bjerknes, J. (1969), Atmospheric Teleconnections from the Equatorial Pacific, *Monthly Weather Review*, 97, 3, 163-172.

Bloom, S., A. da Silva, D. Dee, M. Bosilovich, J-D. Chern, S. Pawson, S. Schubert, M. Sienkiewicz, I. Stajner, W-W. Tan, and M-L. Wu (2005), Documentation and Validation of the Goddard Earth Observing System (GEOS) Data Assimilation System–Version 4, NASA Technical Report Series on Global Modeling and Data Assimilation, editor M. Suarez, NASA/TM—2005–104606, Vol. 26.

Bowman, K. W., T. Steck, H. M. Worden, J. Worden, S. Clough, C. Rodgers (2002), Capturing time and vertical variability of tropospheric ozone: A study using TES nadir retrievals, *J. Geophys. Res.*, 107(D23), 4723, doi:10.1029/2002JD002150.

Bowman, K. W., et al. (2006), Tropospheric Emission Spectrometer: Retrieval method and error analysis, *IEEE Trans. Geosci. Remote Sens.*, 44(5), 1297.

Brasseur, G. P., D. A. Hauglustaine, S. Walters, P. J. Rasch, J. F. Muller, C. Granier, and X. X. Tie (1998), MOZART, a global chemical transport model for ozone and related chemical tracers: 1. Model description, *J. Geophys. Res.*, 103, 28,265–28,289, doi:10.1029/98JD02397.

Chandra, S., J. R. Ziemke, W. Min, and W. G. Read (1998), Effects of 1997–1998 El Niño on tropospheric ozone and water vapor, *Geophys. Res. Lett.*, 25, 3867–3870.

Chandra, S., J. R. Ziemke, P. K. Bhartia, and R. V. Martin (2002), Tropical tropospheric ozone: Implications for dynamics and biomass burning, *J. Geophys. Res.*, 107(D14), 4188, doi:10.1029/2001JD000447.

Chandra, S., J. R. Ziemke, M. R. Schoeberl, L. Froidevaux, W. G. Read, P. F. Levelt, and P. K. Bhartia (2007), Effects of the 2004 El Niño on tropospheric ozone and water vapor, *Geophys. Res. Lett.*, 34, L06802, doi:10.1029/2006GL028779.

Chandra, S., et al. (2009), Effects of the 2006 El Niño on tropospheric ozone and carbon monoxide: Implications for dynamics and biomass burning, *Atmos. Chem. Phys. Disc., 9, 2735-2761*.

Christian, H. J., et al. (1992), The Lightning Imaging Sensor for the Earth Observing System, in Tech Rep. NASA TM-4350, NASA Washington D.C.

Christian, H. J., et al. (1996), The Optical Transient Detector (OTD), in *Proc. 10th Int. Conf. on Atmospheric Electricity*, 368-371, ICAE, Osaka, Japan.

Doherty, R. M., D. S. Stevenson, W. J. Collins and M. G. Sanderson (2005), Influence of convective transport on tropospheric ozone and its precursors in a chemistry-climate model, *Atmos. Chem. Phys.*, 5, 3205-3218.

Duncan, B. N., I. Bey, M. Chin, L. J. Mickley, T. D. Fairlie, R. V. Martin, H. Matsueda (2003a), Indonesian wildfires of 1997: Impact on tropospheric chemistry, *J. Geophys. Res.*, 108(D15), 4458, doi:10.1029/2002JD003195.

Duncan, B. N., R. V. Martin, A. C. Staudt, R. Yevich, and J. A. Logan (2003b), Interannual and seasonal variability of biomass burning emissions constrained by satellite observations, *J. Geophys. Res.*, 108(D2), 4100, doi:10.1029/2002JD002378.

Field, R. D., and S. S. P. Shen (2008), Predictability of carbon emissions from biomass burning in Indonesia from 1997 to 2006, *J. Geophys. Res.*, 113, G04024, doi:10.1029/2008JG000694.

Fujiwara, M., K. Kita, S. Kawakami, T. Ogawa, N. Komala, S. Saraspriya, and A. Suripto (1999), Tropospheric ozone enhancements during the Indonesian forest fire events in 1994 and in 1997 as revealed by ground-based observations, *Geophys. Res. Lett.*, 26(16), 2417-2420.

Giglio L, J. Descloitres J, C. O. Justice, Y. J. Kaufman (2003), An enhanced contextual fire detection algorithm for MODIS, *Remote Sensing of Environment*, 87 (2-3): 273-282.

Guenther et al. (2006), Estimates of global terrestrial isoprene emissions using MEGAN (Model of Emissions of Gases and Aerosols from Nature), *Atmos. Chem. Phys.* 6, 3181-3210.

Hack, J. J. (1994), Parameterization of moist convection in the NCAR community climate model (CCM2), *J. Geophys. Res.*, 99, 5551-5568.

Hamid E. Y., Z.-I Kawasaki, R. Mardiana (2001), Impact of the 1997-98 El Niño Event on Lightning Activity over Indonesia, *Geophys. Res. Lett.*, 28(1), 147-150.

Hauglustaine, D. A., G. P. Brasseur, J. S. Levine (1999), A sensitivity simulation of tropospheric ozone changes due to the 1997 Indonesian fire emissions, *Geophys. Res. Lett.*, 26(21), 3305-3308.

Heimann, M. and M. Reichstein (2008), Terrestrial ecosystem carbon dynamics and climate feedbacks, *Nature*, 451, 289-292, doi:10.1038/nature06591.

Hudman, R. C., D. J. Jacob, S. Turquety, E. M. Leibensperger, L. T. Murray, S. Wu, A. B. Gilliland, M. Avery, T. H. Bertram, W. Brune, R. C. Cohen, J. E. Dibb, F. M. Flocke, A. Fried, J. Holloway, J. A. Neuman, R. Orville, A. Perring, X. Ren, G. W. Sachse, H. B. Singh, A. Swanson, P. J. Wooldridge (2007), Surface and lightning sources of nitrogen oxides over the United States: magnitudes, chemical evolution, and outflow, *J. Geophys. Res.*, 112, D12S05, doi:10.1029/2006JD007912.

Jaeglé, L., R. V. Martin, K. Chance, L. Steinberger, T. P. Kurosu, D. J. Jacob, A. I. Modi, V. Yoboué, L. Sigha-Nkamdjou, and C. Galy-Lacaux (2004), Satellite mapping of rain-induced nitric oxide emissions from soils, *J. Geophys. Res.*, 109, D21310, doi:10.1029/2004JD004787.

Jaeglé, L., L. Steinberger, R.V. Martin and K. Chance (2005), Global partitioning of NO_x sources using satellite observations: Relative roles of fossil fuel combustion, biomass burning and soil emissions, *Faraday Discuss.*, 130, 407–423, doi:10.1039/b502128f.

Jourdain, L., S. S. Kulawik, H. M. Worden, K. E. Pickering, J. Worden, A. M. Thompson (2009) Lightning NO_x emissions over the USA investigated using TES, NLDN, LRLDN, IONS data and the GEOS-Chem model, *Atmos. Chem. Phys. Disc., 9, 1123-1155.*

Keeling, C. D., T. P. Whorf, M. Whalen and J. Vanderplicht (1995), Interannual extremes in the rate of rise of atmospheric carbon-dioxide since 1980, *Nature*, 375, 666-670.

Keeling, C. D. et al., Exchanges of Atmospheric CO_2 and $^{13}CO_2$ with the Terrestrial Biosphere and Oceans from 1978 to 2000. I. Global aspects (Scripps Institution of Oceanography, San Diego, 2001).

Khandekar, M. L., T. S. Murty, D. Scott and W. Baird (2000), The 1997 El Niño, Indonesian forest fires and the Malaysian smoke problem: A deadly combination of natural and man-made hazard, *Nat. Hazards*, 21, 131–144.

Kita, K., M. Fujiwara, S. Kawakami (2000), Total ozone increase associated with forest fires over the Indonesian region and its relation to the El Niño-Southern oscillation, *Atmos. Env.*, 34, 2681-2690.

Klonecki, A., and H. Levy II (1997), Tropospheric chemical ozone tendencies in CO-CH_4-NOy-H_2O system: Their sensitivity to variations in environmental parameters and their application to a global chemistry transport model study, *J. Geophys. Res.*, 102(D17), 21221-21237.

Kuhns, H., M. Green, V. Etyemezian (2003), Big Bend Regional Aerosol and Visibility Observational (BRAVO) Study Emissions Inventory, Report prepared for BRAVO Steering Committee, Desert Research Institute, Las Vegas, Nevada.

Kulawik, S. S., K. W. Bowman, M. Luo, C. D. Rodgers, and L. Jourdain (2008), Impact of nonlinearity on changing the a priori of trace gas profiles estimates from the Tropospheric Emission Spectrometer (TES), *Atmos. Chem. Phys.* 8, 3081-3092.

Langenfelds, R. L., R. J. Francey, B. C. Pak, L. P. Steele, J. Lloyd, C. M. Trudinger and C. E. Allison (2002), Interannual growth rate variations of atmospheric CO_2 and its delta C-13, H_2, CH_4, and CO between 1992 and 1999 linked to biomass burning, *Global Biogeochem. Cycles*, 16, 1048, doi:10.1029/2001GB001466.

Lawrence, M. G. and M. Salzmann (2008), On interpreting studies of tracer transport by deep cumulus convection and its effects on atmospheric chemistry, *Atmos. Chem. Phys.*, 8, 6037-6050.

Lawrence, M. G., R. von Kuhlmann, M. Salzmann and P. J. Rasch, The balance of effects of deep convective mixing on tropospheric ozone, *Geophys. Res. Lett.*, 30(18), 1940, doi:10.1029/2003GL017644, 2003.

Levine, J. (1999), The 1997 fires in Kalimantan and Sumatra, Indonesia: Gaseous and particulate emissions, *Geophys. Res. Lett.*, 26, 815– 818.

Liebmann, B. and C.A. Smith (1996), Description of a Complete (Interpolated) Outgoing Longwave Radiation Dataset, *Bulletin of the American Meteorological Society*, 77, 1275-1277.

Logan, J. A., I. A. Megretskaia, R. Nassar, L. T. Murray, L. Zhang, K. W. Bowman, H. M Worden, M. Luo (2008), Effects of the 2006 El Niño on tropospheric composition as revealed by data from the Tropospheric Emission Spectrometer (TES), *Geophys. Res. Lett.*, 35, L03816, doi:10.1029/2007GL031698.

Lopez, J. P., M. Luo, L. E. Christensen, M. Loewenstein, H. Jost, C. R. Webster, and G. Osterman (2008), TES carbon monoxide validation during two AVE campaigns using the Argus and ALIAS instruments on NASA's WB-57F, *J. Geophys. Res.*, in press doi:10.1029/2007JD008811.

Luo, M., et al. (2007a), Carbon monoxide measurements by TES and MOPITT – the influence of a priori data and instrument characteristics on nadir atmospheric species retrievals, *J. Geophys. Res.*, 112, D09303, doi:101029/2006JD007663.

Luo, M., et al. (2007b), TES carbon monoxide validation with DACOM aircraft measurements during INTEX-B 2006, *J. Geophys. Res.*, 112, D24S48, doi:10.1029/2007JD008803.

Mach, D.M., H. J. Christian, R. J. Blakeslee, D. J. Boccipipio, S. J. Goodman, W. L. Beck (2007), Performance assessment of the Optical Transient Detector and Lightning Imaging Sensor, *J. Geophys. Res.*, 112, D09210, doi:10/29/2006JD007787.

Nassar, R. et al. (2008), Validation of Tropospheric Emission Spectrometer (TES) nadir ozone profiles, *J. Geophys. Res.*, 13, D15S17, doi:10.1029/2007JD008819.

Olivier, J. G. J. and J. J. M. Berdowski (2001), Global emissions sources and sinks. In: Berdowski, J., Guicherit, R. and B.J. Heij (eds.) "The Climate System", pp. 33-78. A. A. Balkema Publishers/Swets and Zeitlinger Publishers, Lisse, The Netherlands.

Page, S. E., F. Siegert, J. O. Rieley, H.-D. V. Boehm, A. Jayak, and S. Limink (2002), The amount of carbon released from peat and forest fires in Indonesia during 1997, *Nature*, 420, 61-65.

Park, R. J., D. J. Jacob, N. Kumar, and R. M. Yantosca (2006), Regional visibility statistics in the United States: Natural and transboundary pollution influences, and implications for the Regional Haze Rule, *Atmos. Environ., 40*(28), 5405-5423.

Pickering, K., Y. Wang, W.-K. Tao, C. Price, and J.-F. Müller (1998), Vertical distributions of lightning NO_x for use in regional and global chemical transport models, *J. Geophys. Res.*, 103(D23), 31203-31216.

Rasmusson, E. M., and J. M. Wallace (1983), Meteorological Aspects of the El Niño/Southern Oscillation, *Science*, 222, 1195-1202.

Richards, N. A. D., G. B. Osterman, E. V. Browell, J. W. Hair, M. Avery, and Q. Li (2008), Validation of Tropospheric Emission Spectrometer ozone profiles with aircraft observations during the Intercontinental Chemical Transport Experiment–B, *J. Geophys. Res.*, 113, D16S29, doi:10.1029/2007JD008815.

Rinsland, C. P., et al. (2006), Nadir measurements of carbon monoxide distributions by the Tropospheric Emission Spectrometer instrument onboard the Aura Spacecraft: Overview of analysis approach and examples of initial results, *Geophys. Res. Lett.*, 33, L22806, doi:10.1029/2006GL027000.

Rinsland, C. P., M. Luo, M. W. Shephard, C. Clerbaux, C. Boone, P. F. Bernath, L. Chiou, P. F. Coheur (2008), Tropospheric emission spectrometer (TES) and Atmospheric Chemistry Experiment (ACE) measurements of tropospheric chemistry in tropical southeast Asia during a moderate El Niño in 2006, *J. Quant. Spectrosc. Radiat. Trans.*, 109, 1931-1942, doi:10.1016/j.jqsrt.2007.12.020.

Rodgers, C. D. (2000), Inverse Methods for Atmospheric Sounding: Theory and Practice, World Scientific, London.

Saji, N. H., B. N. Goswami, P. N. Vinayachandran, T. Yamagata (1999), A dipole mode in the tropical Indian Ocean, *Nature*, 401, 360-363.

Sauvage, B., R. V. Martin, A. van Donkelaar, X. Liu, K. Chance, L. Jaeglé, P. I. Palmer, S. Wu, T.-M. Fu (2007a), Remote sensed and in situ constraints on processes affecting tropical tropospheric ozone, *Atmos. Chem. Phys.*, 7, 815-838.

Sauvage, B., R. V. Martin, A. van Donekelaar, J. R. Ziemke (2007b), Quantification of the factors controlling tropical tropospheric ozone and the South Atlantic maximum, *J. Geophys. Res.*, 112, D11309, doi:10.1029/2006JD008008.

Shein, K. A., et al. (2006), State of the climate, 2005, *Bull. Am. Met. Soc., 87,* S6-S102.

Shephard, M. W., et al. (2008), Comparison of Tropospheric Emission Spectrometer (TES) water retrievals with in situ measurements, *J. Geophys. Res.*, 113, D15S24, doi:10.1029/2007JD008822.

Stajner, I., et al. (2008), Assimilated ozone from EOS-Aura: Evaluation of the tropopause region and tropospheric columns, *J. Geophys. Res.*, 113, D16S32, doi:10.1029/2007JD008863.

Streets, D. G., T. C. Bond, G. R. Carmichael, S. D. Fernandes, Q. Fu, Z. Klimont, S. M. Nelson, N. Y. Tsai, M. Q. Wang, J-H. Woo, and K. F. Yarber (2003), An inventory of gaseous and primary aerosol emissions in Asia in the year 2000, *J. Geophys. Res*., 108, D21, doi:10.1029/2002JD003093.

Streets, D. G, Q. Zhang, L. Wang, K. He, J. Hao, Y. Wu, Y. Tang, and G. C. Carmichael (2006), Revisiting China's CO emissions after the Transport and Chemical Evolution over the Pacific (TRACE-P) mission: Synthesis of inventories, atmospheric modeling, and observations, *J. Geophys. Res*., 111, D14306, doi:10.1029/2006JD007118.

Sudo, K. and M. Takahashi (2001), Simulation of tropospheric ozone changes during 1997-1998 El Niño: Meteorological impact on tropospheric photochemistry, *Geophys. Res. Lett.*, 28(21), 4091-4094.

Thompson, A. M., J. C. Witte, R. D. Hudson, H. Guo, J. R. Herman, M. Fujiwara (2001), Tropical Tropospheric Ozone and Biomass Burning, *Science*, 291, 2128-2132.

Thompson, A. M., J. C. Witte, R. D. McPeters, S. J. Oltmans, F. J. Schmidlin, J. A. Logan, M. Fujiwara, V. W. J. H. Kirchhoff, F. Posny, G. J. R. Coetzee, B. Hoegger, S. Kawakami, T. Ogawa, B. J. Johnson, H. Vömel, G. Labow (2003), Southern Hemisphere Additional Ozonesondes (SHADOZ) 1998-2000 tropical ozone climatology. 1. Comparison with TOMS and ground-based measurements, *J. Geophys. Res.*, 108, 8238, doi:10.1029/2001JD000967.

Thompson, A. M., J. C. Witte, H. G. J. Smit, S. J. Oltmans, B. J. Johnson, V. W. J. H. Kirchhoff, F. J. Schmidlin (2007), Southern Hemisphere Additional Ozonesondes (SHADOZ) 1998-2004

tropical ozone climatology. 3. Instrumentation, Station Variability, Evaluation with Simulated Flight Profiles, *J. Geophys. Res.*, 112, D03304, doi:10.1029/2005JD007042.

van der Werf, G. R., J. T. Randerson, L. Giglio, G. J. Collatz, P. S. Kasibhatla, and A. F. Arellano Jr. (2006), Interannual variability in global biomass burning emissions from 1997 to 2004, *Atmos. Chem. Phys.*, 6, 3423-3441.

van der Werf, G. R., J. Randerson, L. Giglio, N. Gobron, and H. Dolman (2008), Climate controls on the variability of fires in the tropics and subtropics, *Global Biogeochem. Cycles*, 22, GB3028, doi:10.1029/2007GB003122.

van Donkelaar, A., et al. (2008), Analysis of aircraft and satellite measurements from the Intercontinental Chemical Transport Experiment (INTEX-B) to quantify long-range transport of East Asian sulfur to Canada, *Atmos. Chem. Phys.*, 8, 2999–3014.

Vestreng, V., and H. Klein (2002), Emission data reported to UNECE/EMEP: Quality assurance and trend analysis and Presentation of WebDab, MSC-W Status Report 2002, Norwegian Meteorological Institute, Oslo Norway, July 2002.

Wang, Y., D. J. Jacob, J. A. Logan (1998), Global simulation of tropospheric O_3-NO_x-hydrocarbon chemistry: 1. Model formulation, *J. Geophys. Res.*, 103(D9), 10713-10725.

Webster, P. J., A. M. Moore, J. P. Loschnigg, and R.R. Leben (1999) Coupled ocean-atmosphere dynamics in the Indian Ocean during 1997-98, *Nature*, 40, 356-360.

Worden, J. S., S. S. Kulawik, M. Shepard, S. Clough, H. Worden, K. Bowman, A. Goldman (2004), Predicted errors of Tropospheric Emission Spectrometer nadir retrievals from spectral window selection, *J. Geophys. Res.*, 109, D09308, doi:10.1029/2004JD004522.

Worden, H. M., et al. (2007), Comparisons of Tropospheric Emission Spectrometer (TES) ozone profiles to ozonesondes: Methods and initial results, *J. Geophys. Res.*, 112, D03309, doi:10.1029/2006JD007258.

Yamaguchi, K., and A. Noda (2006), Global warming patterns over the North Pacific: ENSO vs. AO, *Journal of the Meteorological Society of Japan*, 84(1), 221-241.

Yevich, R., and J. A. Logan (2003), An assessment of biofuel use and burning of agricultural waste in the developing world, *Global Biogeochem. Cycles*, 17(4), 1095, doi:10.1029/2002GB001952.

Yienger, J. J., H. Levy II (1995), Empirical model of global soil-biogenic NO_x emissions, *J. Geophys. Res.*, 100(D6), 11447-11464.

Yurganov, L. N., W. W. McMillan, A. V. Dzhola, E. I. Grechko, N. B. Jones, G. R. van der Werf (2008), Global AIRS and MOPITT CO measurements: Validation, comparison, and links to

biomass burning variations and carbon cycle, *J. Geophys. Res.*, 113, D09301, doi:10.1029/2007JD009229.

Zhang, G. J., and N. A. McFarlane (1995), Sensitivity of climate simulations to the parameterization of cumulus convection in the Canadian Climate Centre General Circulation Model, *Atmos. Ocean*, 33, 407– 446.

Zhang, L., et al. (2006), Ozone-CO correlations determined by the TES satellite instrument in continental outflow regions, *Geophys. Res. Lett.*, 33, L18804, doi:10.1029/2006GL026399.

Ziemke, J. R., S. Chandra and P. K. Bhartia (1998), Two new methods for deriving tropospheric column ozone from TOMS measurements: Assimilated UARS MLS/HALOE and convective-cloud differential techniques, *J. Geophys. Res.*, 103(D17), 22,115-22,127.

Ziemke, J. R. and S. Chandra (2003), La Nina and El Niño-induced variabilities of ozone in the tropical lower atmosphere during 1970-2001, *Geophys. Res. Lett.*, 30(3), 1142-1145.

Figure Captions

Figure 1: Lower tropospheric (LT, 825-511 hPa) CO, O_3 and H_2O for October, November and December 2006 from TES (left column), the GEOS-Chem *Base* run (GEOS-4 for H_2O) with the TES averaging kernel applied (middle column), and the model wAK – TES difference (right column).

Figure 2: Comparison between GEOS-Chem O_3 profiles (dashed lines) from the *Base* run and ozonesonde measurements (solid lines) at Java, Kuala Lumpur (KL) and Samoa during the relevant months of 2005 and 2006. The *ScldLight-3xE* run (dotted lines) is also shown for the October to December 2006 plots and lies close to the *Base* run profiles.

Figure 3: LT CO, O_3 and H_2O 2006-2005 differences or anomalies from TES and the GEOS-Chem *Base* run (GEOS-4 for H_2O) wAKs for October, November and December.

Figure 4: CO and O_3 anomalies based on GEOS-Chem *2006e05* wAK (2006 runs using 2005 GFED emissions) minus 2005 *Base*. The primary CO anomaly from Figure 3 is no longer seen, while the main O_3 anomaly from Figure 3 is still present but reduced in size (especially in November) and shifted south of the equator.

Figure 5: CO from TES and the GEOS-Chem *Base* run wAK shown on half-month intervals for October and November 2006 (Table 2 gives exact time periods). The rectangle denotes the 5ºN-11ºS, 91.25-121.25ºW region of the LT which is averaged for time series line plots (Figures 6 and 11). The dramatic change in CO between the first and last half of November is evident.

Figure 6: The time evolution of TES and the GEOS-Chem *Base* run for CO, O_3 and H_2O in late 2005 and 2006. GFED CO emissions are shown corresponding to the axis on the right. The GEOS-Chem *2006e05* and *3xE* runs are also shown. All values are half-month means plotted at 0.25 and 0.75 of each month and the TES averaging kernel has been applied to the model data.

Figure 7: GFED CO emissions (2ºx2.5º resolution) originating from the region of Indonesia and New Guinea (top panel). Regional CO emissions from 2005 and 2006 are plotted on the 4th day of each 8-day interval (2nd panel). Precipitation at Palangkaraya and Banjarmasin in late 2006 (from http://www.tutiempo.net, lower panels).

Figure 8: Separating the effects of emissions and meteorology. The left column shows the total monthly 2006-2005 anomalies for the LT calculated from the *3xE* GEOS-Chem run for 2006 (increased biomass burning emissions in November 2006) and the Base run for 2005. The middle column shows the contribution directly from the *3xE* biomass burning enhancement in 2006 relative to 2005 biomass burning emissions (2006 3xE – 2006 E05). The right column shows the contribution to the anomaly from other factors (2006 E05 – 2005 base, which is also the difference of the other two columns) and is equivalent to the right column in Figure 4.

Figure 9: GEOS-Chem 2006 lightning flash rate (left), GEOS-Chem 2006-2005 lightning anomalies (middle), and Lightning Imaging Sensor (LIS) lightning anomalies (right), both in percent. The rectangle shows the region (9ºN-13ºS and 93.75-151.25ºE) for which model lightning is too low necessitating an increase.

Figure 10: Net O_3 from lightning in the UT and LT for October-December determined by taking the difference between ozone in *Base-13* minus *NoLight* for 2005 (left) and 2006 (middle). The 2006-2005 difference between the *NoLight* runs (right) shows a strong resemblance to the overall O_3 anomaly in Figure 3.

Figure 11: Time evolution of O_3 from TES and the GEOS-Chem *Base*, *3xE*, *ScldLight*, *ScldLight-3xE* and *SoilNOx10* runs for the UT and LT (upper and middle panels). The TES averaging kernel has been applied to the model data. GEOS-4 updraft mass fluxes for model sigma levels near 10 km (multiplied by 4) and 6.6 km are also shown with GEOS-4 and NOAA Outgoing Longwave Radiation (OLR) (bottom panel). The GEOS-4 data correspond to the same region (11ºS-5ºN, 91.25-121.25ºE) region as the TES and GEOS-Chem data, but the NOAA OLR averages are for a slightly different region (11.25ºS-6.25ºN, 91.25-121.25ºE) due to its different grid. All values are half-month means plotted at 0.25 and 0.75 of each month.

Figure 12: GEOS-4 horizontal winds at 700 hPa for half-month intervals in 2006.

Figure 13: CO and O_3 contributions from convection in GEOS-Chem, determined as the *Base* run minus *NoConvection* run. Panels show model levels near the base of the tropopause (top row), in the UT (second row), LT (third row) and boundary layer (bottom row) for the first and second halves of November 2006. Approximate altitudes corresponding to GEOS-4 sigma levels are given on the right.

Figure 14: Differences in OLR (2006-2005) from GEOS-4 and NOAA data for October to December in half-month intervals.

Figure 15: GEOS-4 – NOAA OLR for November-December 2006 after applying a bias correction of 13 W/m^2 to account for differences between the OLR datasets (see Figure 11).

Figure 16: Ozone change resulting from an increase in soil NO_x emissions by a factor of 10, for the first and second halves of November near the base of the tropopause, UT, LT and BL. The change was calculated from the difference of *SoilNOx10 – Base*. Approximate altitudes corresponding to GEOS-4 sigma levels are given on the right.

Tables

Table 1: Summary of GEOS-Chem simulations[a.]

Run-name Abbreviation	Description	Date range
Spin	Initialization	20041201 - 20050831
Base	Baseline run (using modified version 7-04-10)	20050901 - 20061231
2006e05	Run with 2005 GFED emissions	20060101 - 20061231
3xE	Run with November GFED emissions increased by a factor of 3 in a box region	20061101 - 20061231
ScldLight	Run with monthly scaled lightning in a box region	20061001 - 20061231
ScldLight-3xE	Run with bi-monthly scaled lightning in a box region and increased November GFED emissions	20061001 - 20061231
NoConvection	Run with deep convection turned off, with each half-month initialized from the baseline run	20061101 - 20061115 20061116 - 20061130 20061201 - 20061215 20061216 - 20061231
Base-13	Baseline run with v7-04-13	20050901 - 20051231 20060901 - 20061231
NoLight	Run with global lightning turned off (v7-04-13)	20050901 - 20051231 20060901 - 20061231
SoilNOx10	Run with soil NO_x emissions increased by a factor of 10 in a box region	20061101 - 20061130

[a] Simulations used a modified version 7-04-10 unless otherwise stated.

1224 Table 2: Nominal half-month periods[a]

1225

Nominal Period	*Exact TES date-time span*	*Global Surveys*
200509 1st half	Sep 02 (8:40:25) – Sep 13 (11:38:57)	6
200509 2nd half	Sep 30 (9:04:58) – Oct 01 (11:26:18)	1
200510 1st half	Oct 02 (8:52:35) – Oct 15 (11:38:49)	7
200510 2nd half	Oct 16 (9:05:08) – Oct 31 (11:39:05)	8
200511 1st half	Nov 05 (8:40:44) – Nov 16 (11:39:15)	6
200511 2nd half	Nov 17 (9:05:34) – Nov 29 (23:17:40)	6.25 [b]
200512 1st half	Dec 07 (8:40:52) – Dec 16 (11:51:36)	5
200512 2nd half	Dec 17 (9:17:54) – Dec 30 (12:03:49)	7
200609 1st half	Sep 09 (9:59:00) – Sep 16 (11:41:55)	4
200609 2nd half	Sep 17 (9:09:35) – Sep 30 (11:34:16)	5
200610 1st half	Oct 01 (9:21:56) – Oct 16 (11:54:09)	8
200610 2nd half	Oct 17 (9:21:49) – Nov 01 (11:53:58)	8
200611 1st half	Nov 02 (9:21:37) – Nov 15 (12:06:06)	7
200611 2nd half	Nov 16 (9:33:44) – Dec 01 (12:05:47)	8
200612 1st half	Dec 02 (9:33:27) – Dec 15 (11:33:56)	7
200612 2nd half	Dec 16 (9:45:55) – Dec 29 (12:30:37)	7

1226 [a] The half-month periods were chosen to balance the need to increase temporal resolution and have
1227 adequate spatial coverage, without dividing Global Surveys.

1228 [b] The final GS for this time period was interrupted on Nov 29 after less than 7 of the required 26 hours.
1229 Warm-up of the TES optical bench (for decontamination) occurred in the gap from Nov. 29 to Dec. 7.

1230

Table 3: Contribution from biomass burning to the 2006-2005 O_3 anomaly in the region of high CO, the TES and model anomalies, and their difference[a].

	Biomass Burning (%)[b]		GC Total Anomaly (ppb)[c]		TES Total Anomaly (ppb)[d]		GC-TES (ppb)	
	LT	**UT**	**LT**	**UT**	**LT**	**UT**	**LT**	**UT**
September 1-15	25	26	8.3	9.6	13.4	14.3	-5.1	-4.7
September 16-30	61	75	5.3	3.8	7.1	0.9	-1.8	+3.0
October 1-15	44	48	16.9	16.3	17.8	15.4	-1.0	+0.9
October 16-31	49	48	18.3	20.7	16.8	23.2	+1.5	-2.5
November 1-15	69	79	13.8	13.9	11.7	16.6	+2.1	-2.7
November 16-30	47	46	9.8	11.8	13.6	16.5	-3.8	-4.7
December 1-15	11	12	11.3	14.2	16.1	18.6	-4.8	-4.4
December 16-31	9	9	4.0	5.2	8.1	9.1	-4.0	-3.9
Mean	**39.4**	**42.9**	**11.0**	**11.9**	**13.1**	**14.3**	**-2.1**	**-2.4**

[a] Results are given for the region 11ºS-5ºN and 91.25-121.25ºE (box in Figure 5)

[b] Based on (2006 *3xE – 2006e05*) relative to the model total

[c] GEOS-Chem total is based on (2006 *3xE-ScldLight* – 2005 *Base*)

[d] Based on the bias-corrected TES O_3 anomaly

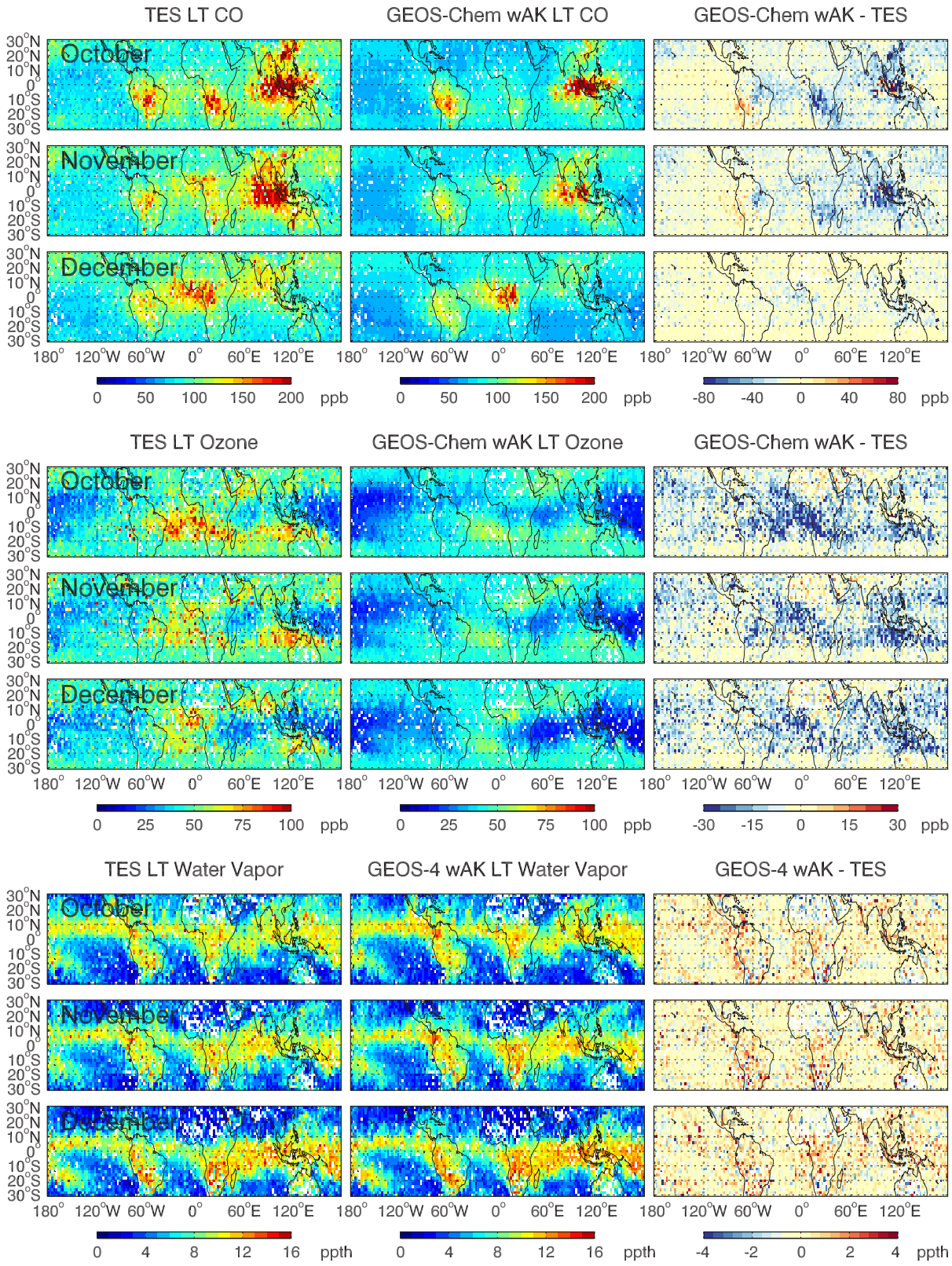

Figure 1: Lower tropospheric (LT, 825-511 hPa) CO, O_3 and H_2O for October, November and December 2006 from TES (left column), the GEOS-Chem *Base* run (GEOS-4 for H_2O) with the TES averaging kernel applied (middle column), and the model wAK – TES difference (right column).

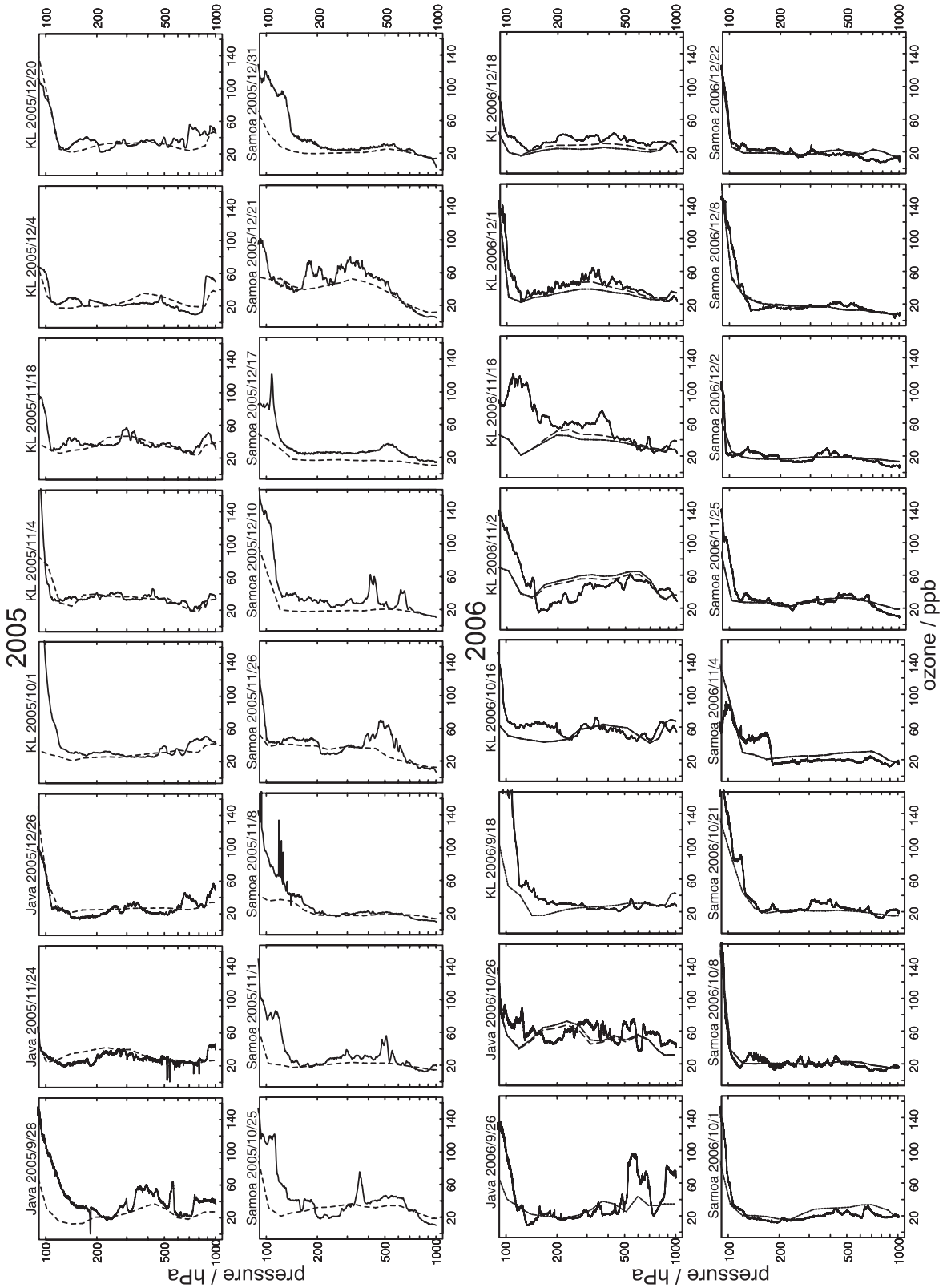

Figure 2: Comparison between GEOS-Chem O_3 profiles (dashed lines) from the *Base* run and ozonesonde measurements (solid lines) at Java, Kuala Lumpur (KL) and Samoa during the relevant months of 2005 and 2006. The *ScldLight-3xE* run (dotted lines) is also shown for the October to December 2006 plots and lies close to the *Base* run profiles.

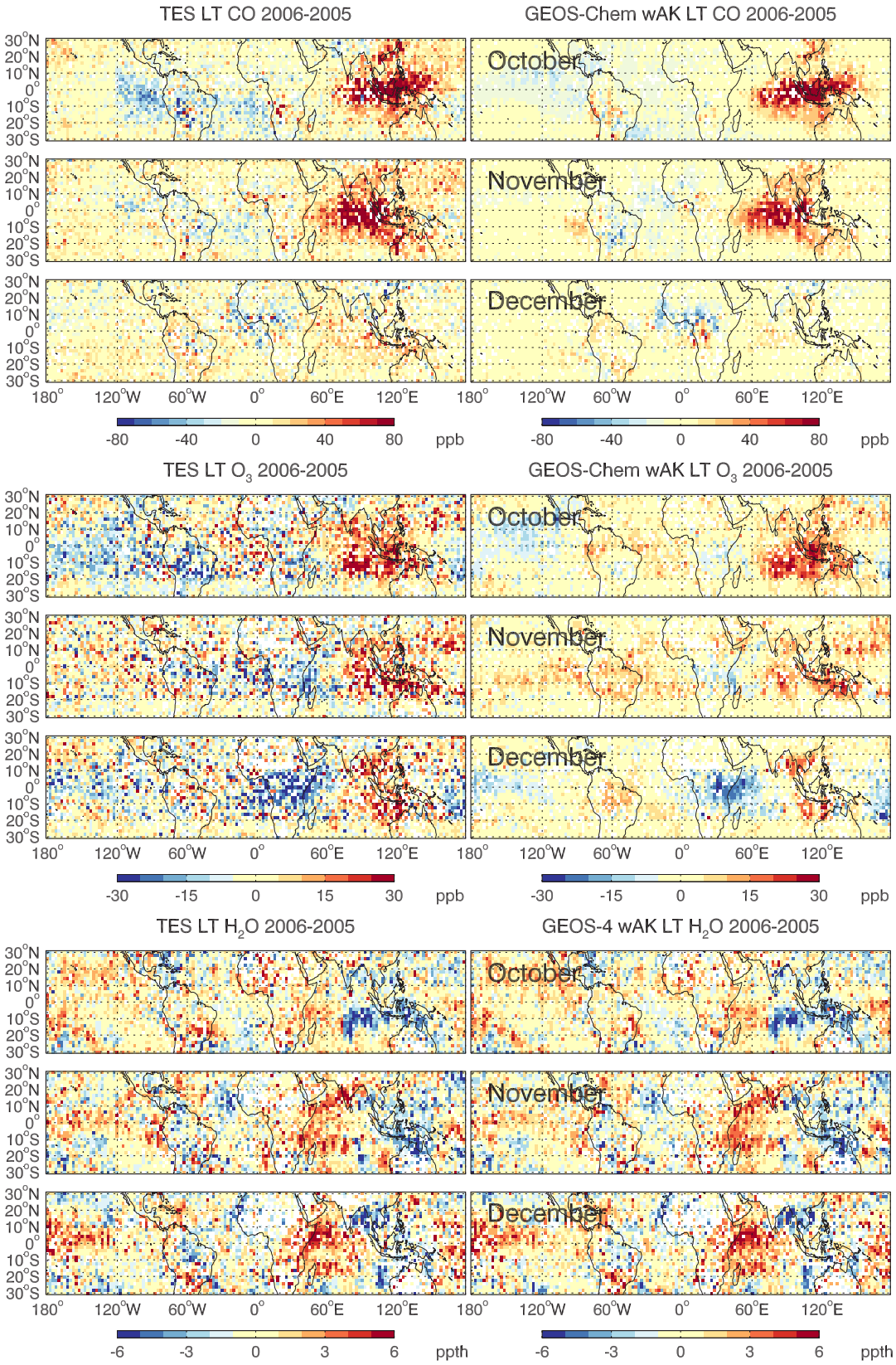

Figure 3: LT CO, O_3 and H_2O 2006-2005 differences or anomalies from TES and the GEOS-Chem *Base* run (GEOS-4 for H_2O) wAKs for October, November and December.

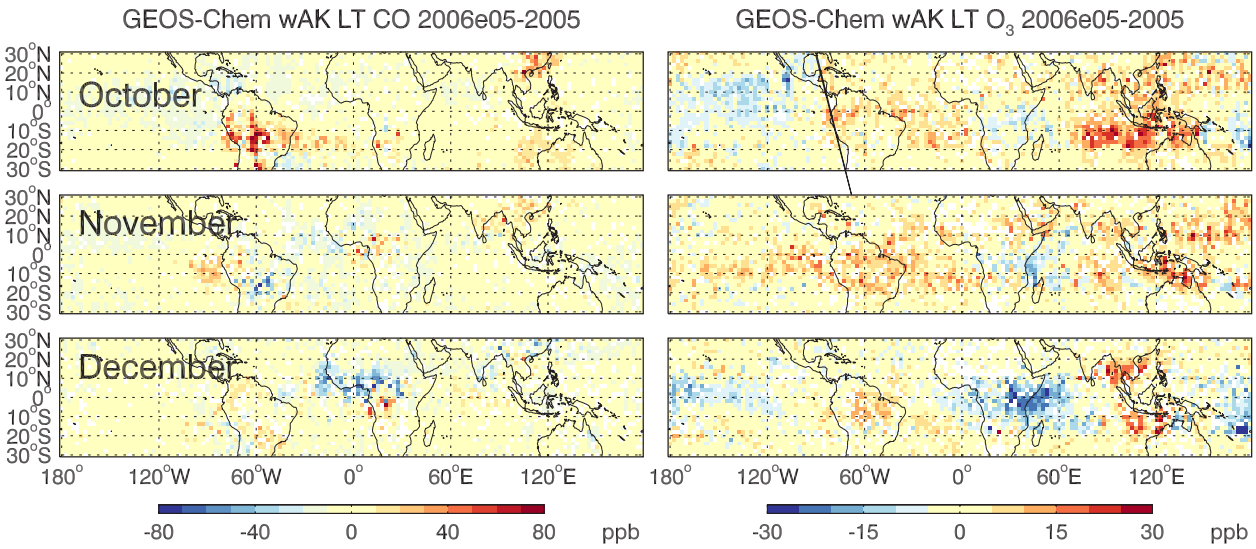

Figure 4: CO and O_3 anomalies based on GEOS-Chem *2006e05* wAK (2006 runs using 2005 GFED emissions) minus 2005 *Base*. The primary CO anomaly from Figure 3 is no longer seen, while the main O_3 anomaly from Figure 3 is still present but reduced in size (especially in November) and shifted south of the equator.

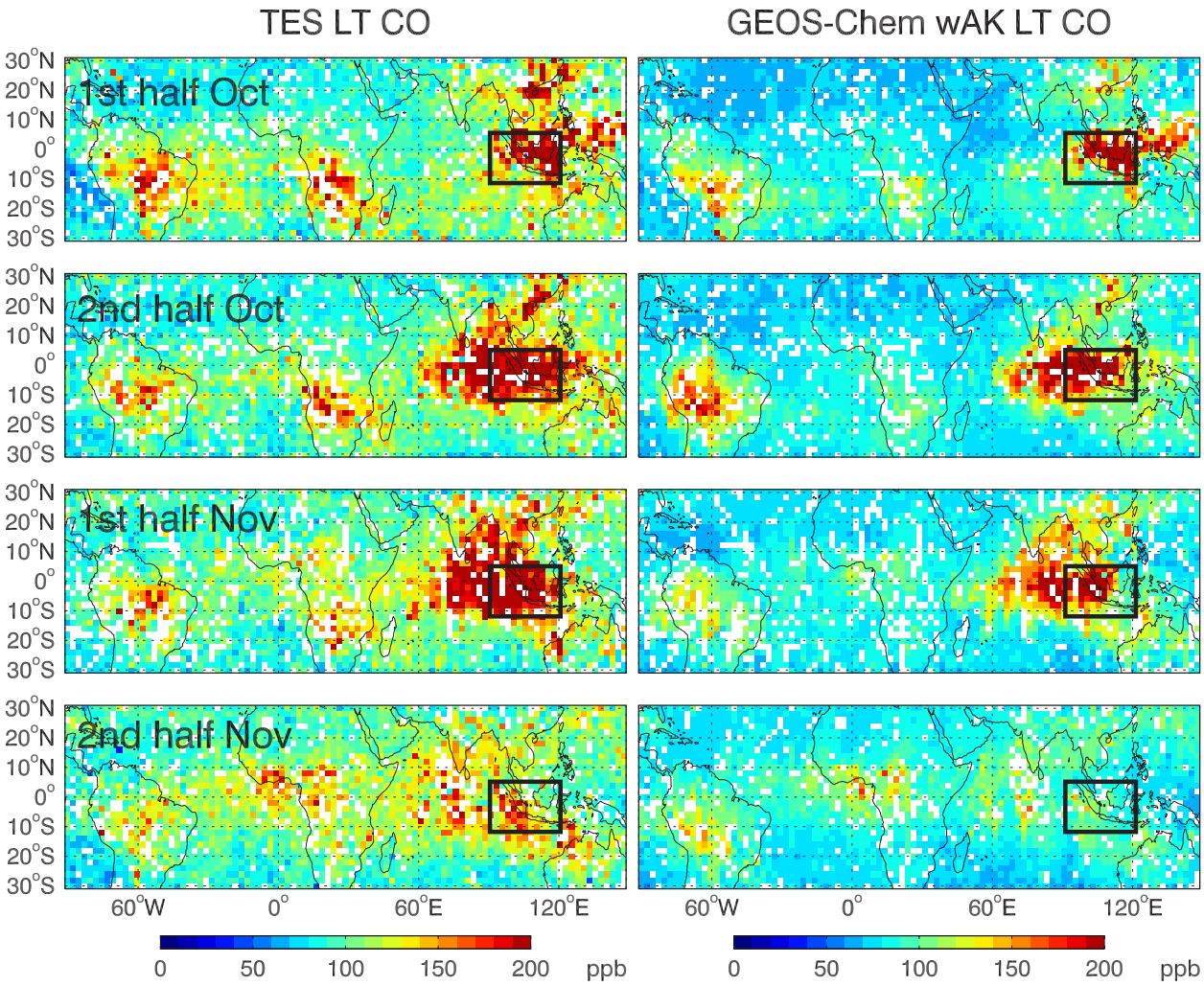

Figure 5: CO from TES and the GEOS-Chem *Base* run wAK shown on half-month intervals for October and November 2006 (Table 2 gives exact time periods). The rectangle denotes the 5ºN-11ºS, 91.25-121.25ºW region of the LT which is averaged for time series line plots (Figures 6 and 11). The dramatic change in CO between the first and last half of November is evident.

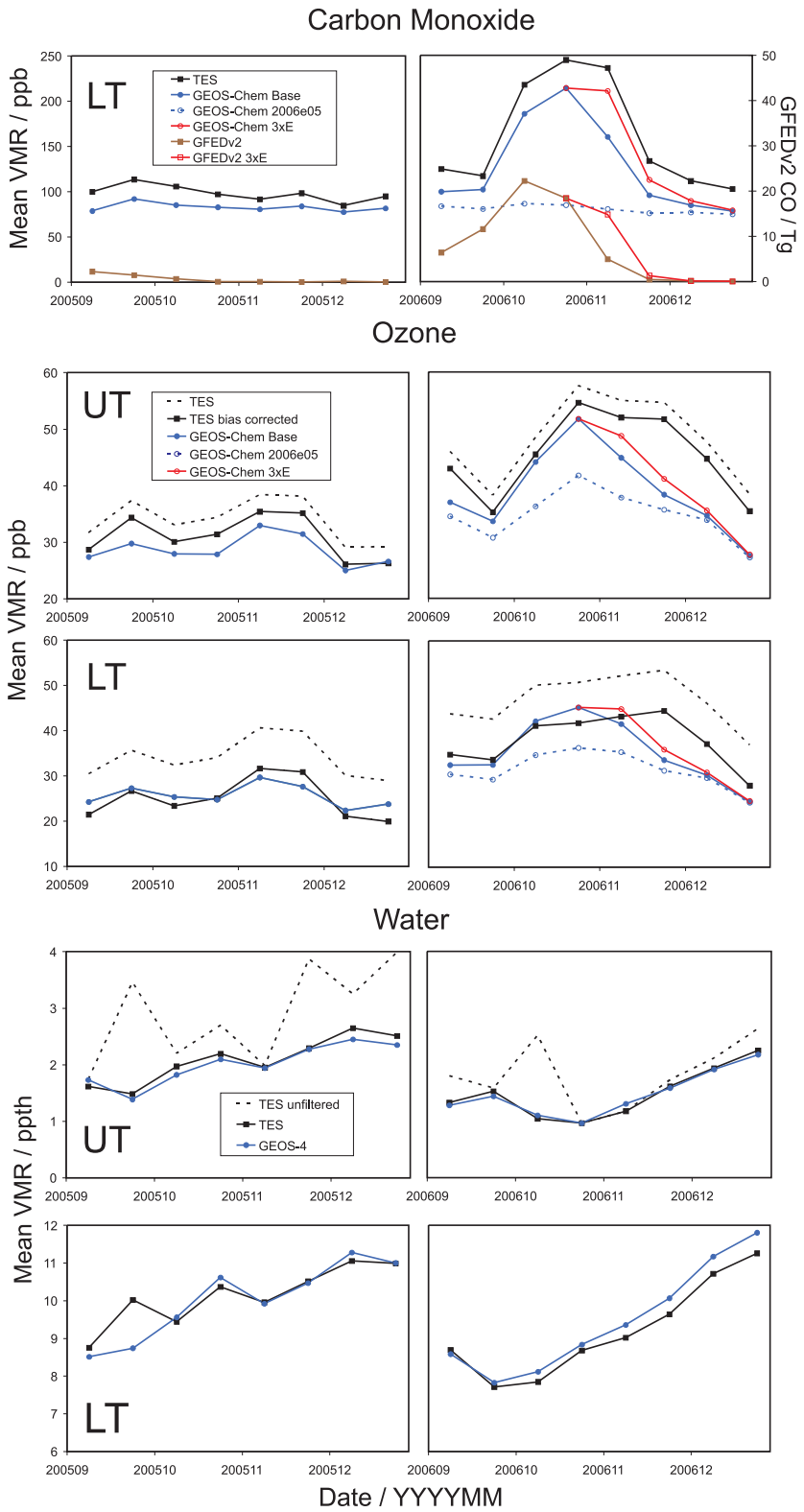

Figure 6: The time evolution of TES and the GEOS-Chem *Base* run for CO, O_3 and H_2O in late 2005 and 2006. GFED CO emissions are shown corresponding to the axis on the right. The GEOS-Chem *2006e05* and *3xE* runs are also shown. All values are half-month means plotted at 0.25 and 0.75 of each month and the TES averaging kernel has been applied to the model data.

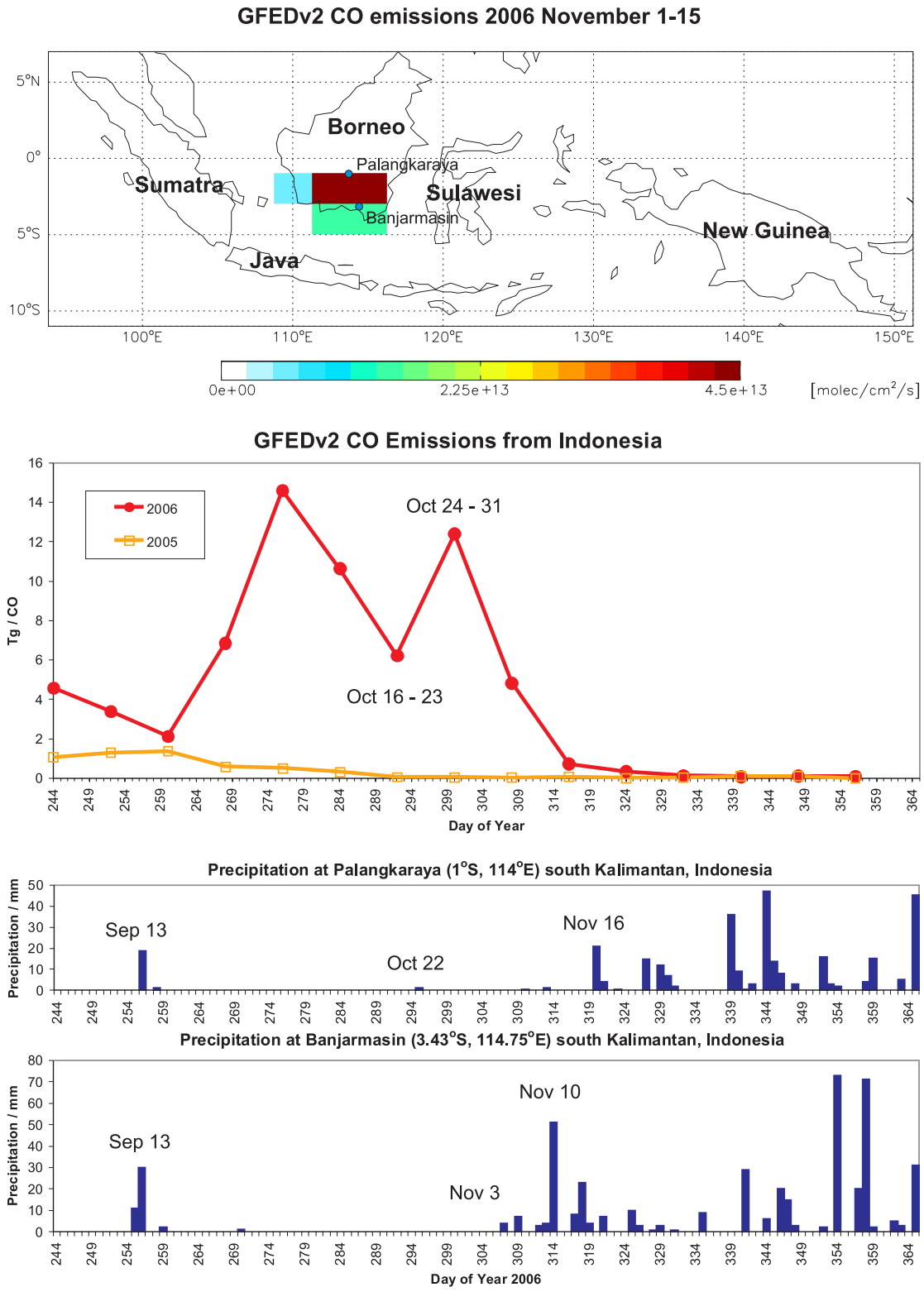

Figure 7: GFED CO emissions (2ºx2.5º resolution) originating from the region of Indonesia and New Guinea (top panel). Regional CO emissions from 2005 and 2006 plotted on the 4th day of each 8-day interval (2nd panel). Precipitation at Palangkaraya and Banjarmasin in late 2006 (from http://www.tutiempo.net, lower panels).

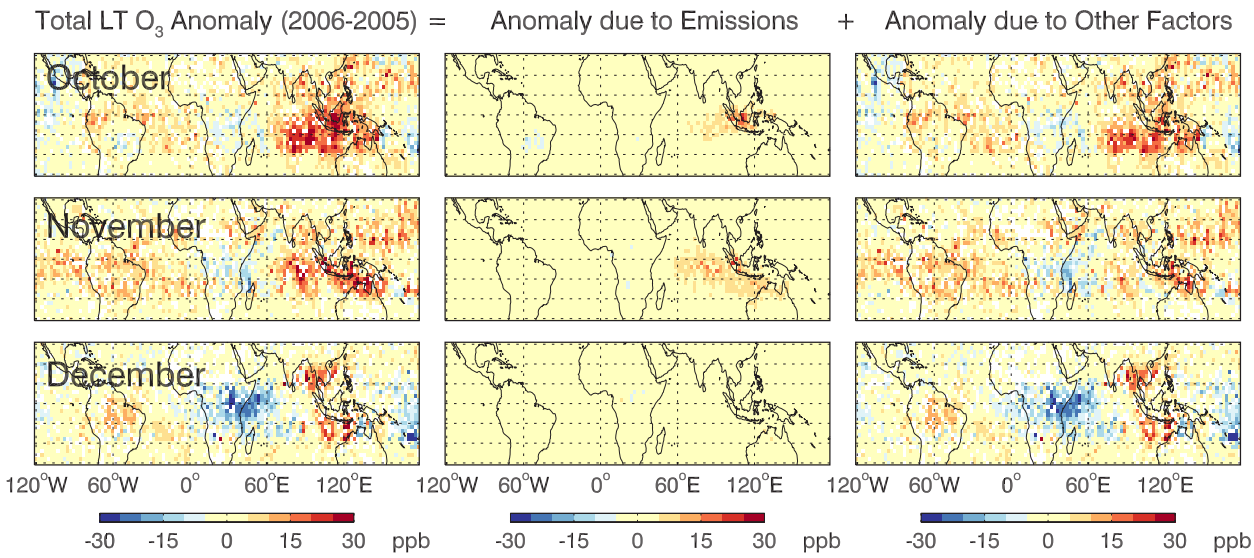

Figure 8: Separating the effects of emissions and meteorology. The left column shows the total monthly 2006-2005 anomalies for the LT calculated from the *3xE* GEOS-Chem run (increased biomass burning emissions in November 2006) and the *Base* run for 2005. The middle column shows the contribution directly from the *3xE* biomass burning enhancement in 2006 relative to 2005 biomass burning emissions (2006 *3xE* – *2006e05*). The right column shows the contribution to the anomaly from other factors (*2006e05* – 2005 *Base*, which is also the difference of the other two columns) and is equivalent to the right column in Figure 4.

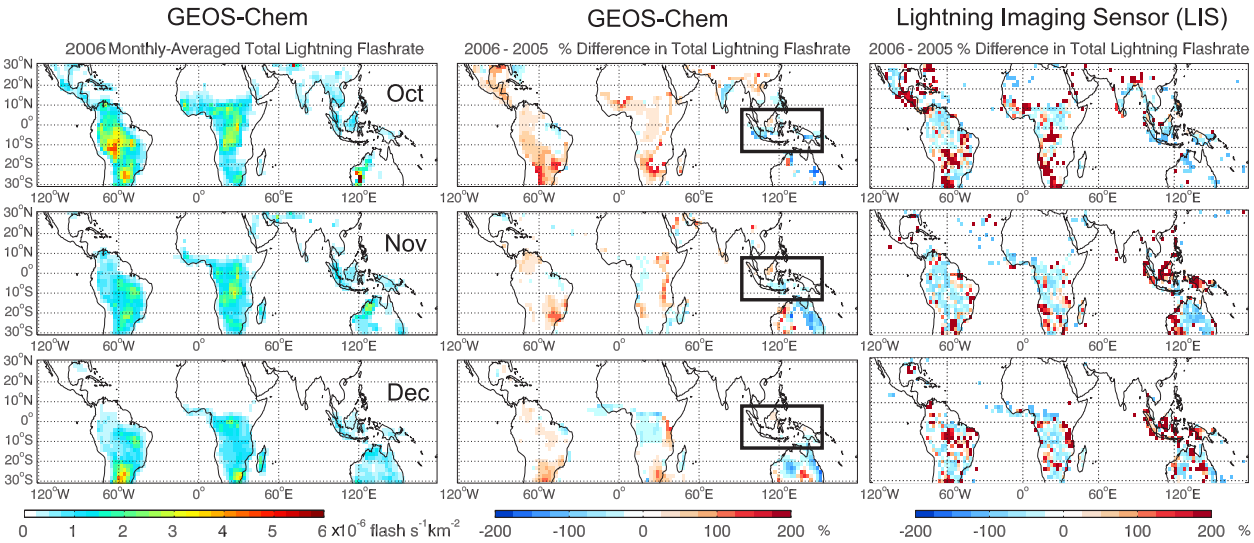

Figure 9: GEOS-Chem 2006 lightning flash rate (left), GEOS-Chem 2006-2005 lightning anomalies (middle), and Lightning Imaging Sensor (LIS) lightning anomalies (right) both in percent. The rectangle shows the region (9ºN-13ºS and 93.75-151.25ºE) for which model lightning is too low necessitating an increase.

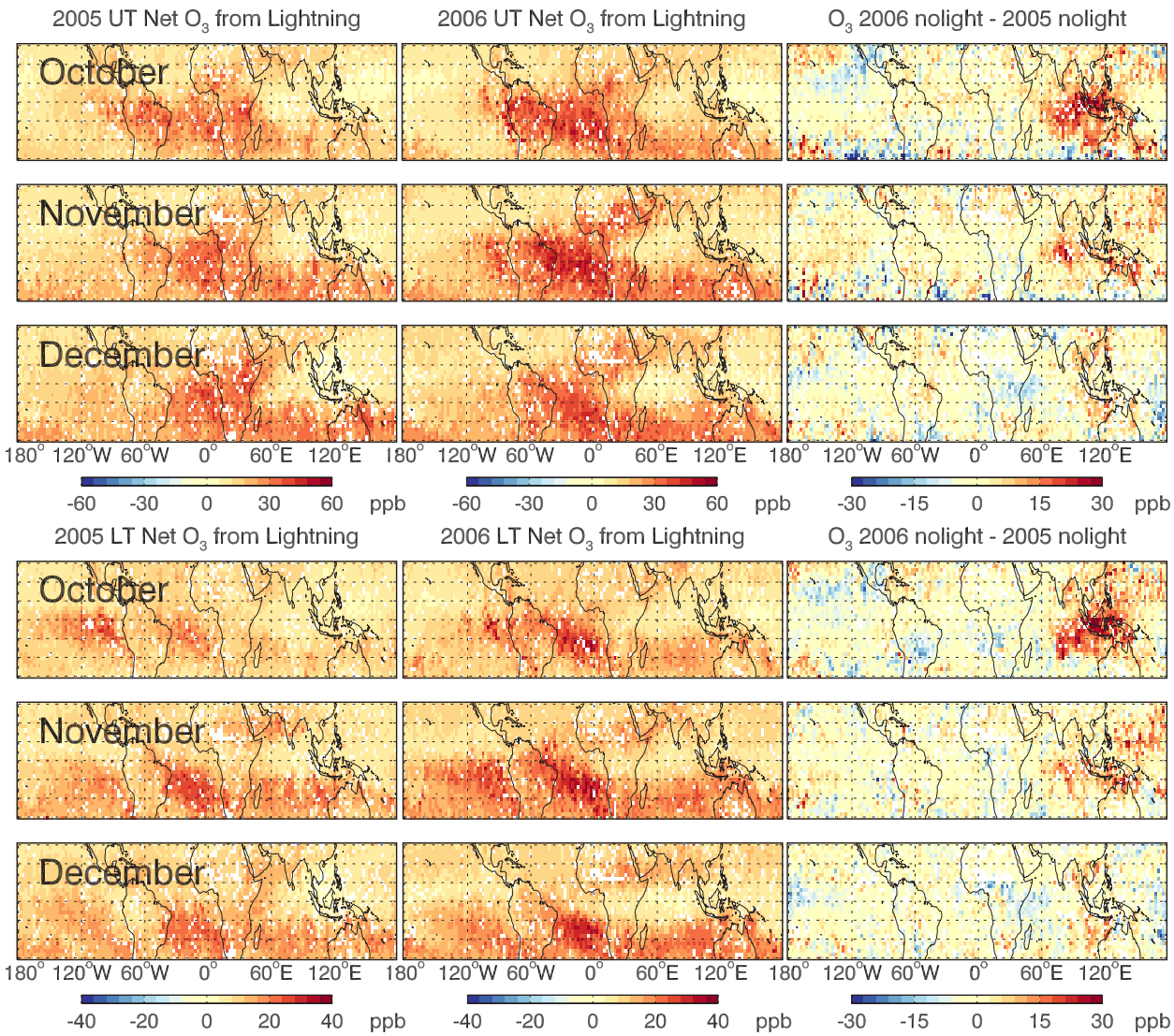

Figure 10: Net O_3 from lightning in the UT and LT for October-December determined by taking the difference between ozone in *Base-13* minus *NoLight* for 2005 (left) and 2006 (middle). The 2006-2005 difference between the *NoLight* runs (right) shows a strong resemblance to the overall ozone anomaly in Figure 3.

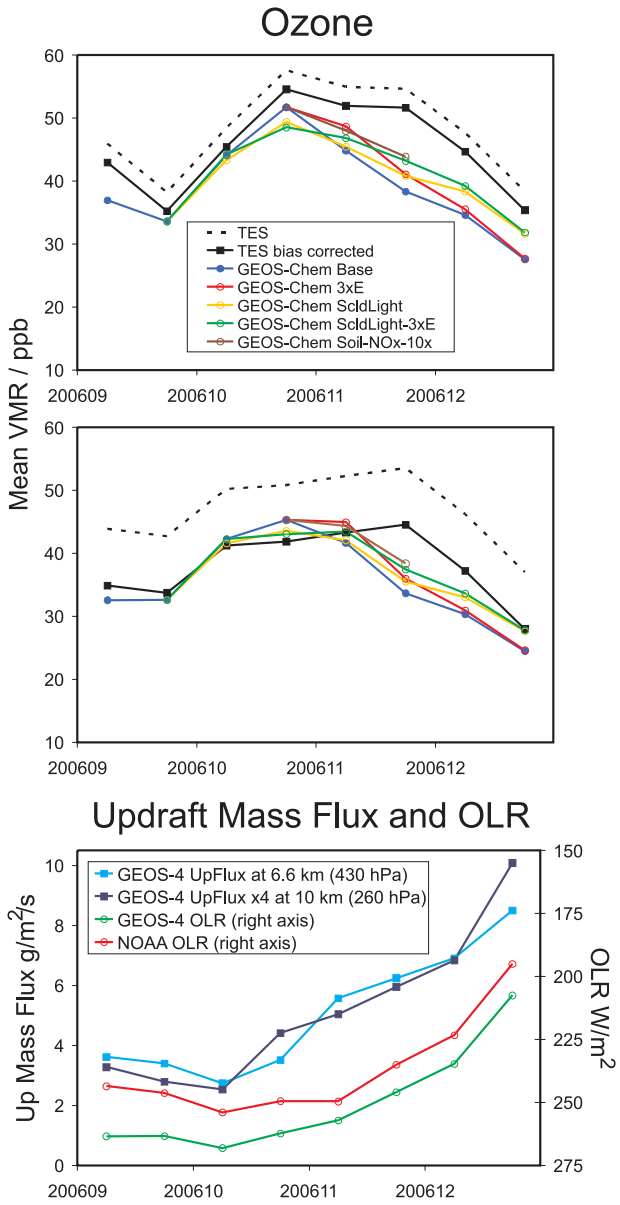

Figure 11: Time evolution of O_3 from TES and the GEOS-Chem *Base*, *3xE*, *ScldLight*, *ScldLight-3xE* and *SoilNO$_x$10* runs for the UT and LT (upper and middle panels). The TES averaging kernel has been applied to the model data. GEOS-4 updraft mass fluxes for model sigma levels near 10 km (multiplied by 4) and 6.6 km are also shown with GEOS-4 and NOAA Outgoing Longwave Radiation (OLR) (bottom panel). The GEOS-4 data correspond to the same region (11ºS-5ºN, 91.25-121.25ºE) as the TES and GEOS-Chem data, but the NOAA OLR averages are for a slightly different region (11.25ºS-6.25ºN, 91.25-121.25ºE) due to its different grid. All values are half-month means plotted at 0.25 and 0.75 of each month.

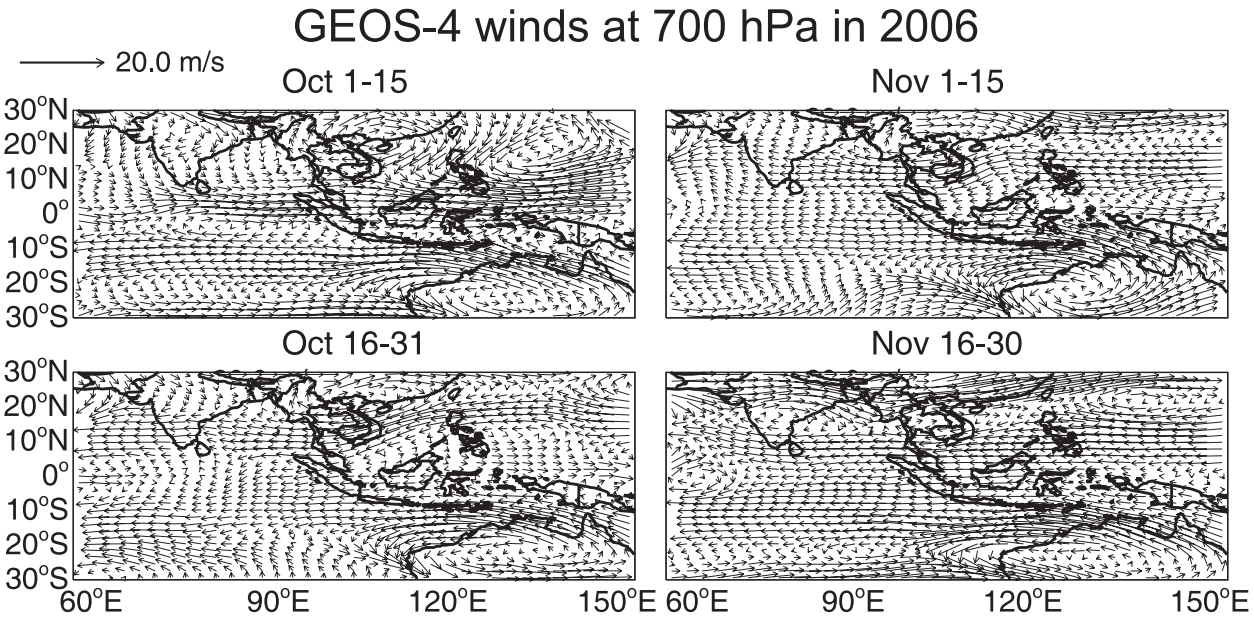

Figure 12: GEOS-4 horizontal winds at 700 hPa for half-month intervals in 2006.

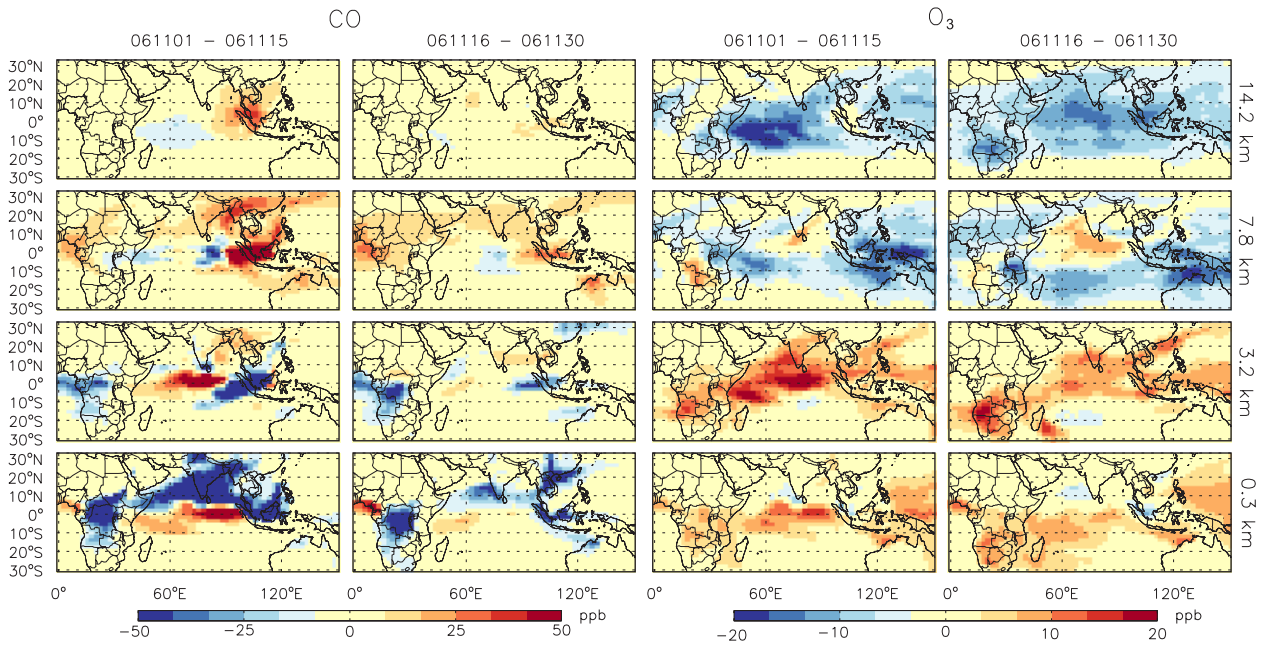

Figure 13: CO and O_3 contributions from convection in GEOS-Chem, determined as the *Base* run minus *NoConvection* run. Panels show model levels near the base of the tropopause (top row), in the UT (second row), LT (third row) and boundary layer (bottom row) for the first and second halves of November 2006. Approximate altitudes corresponding to GEOS-4 sigma levels are given on the right.

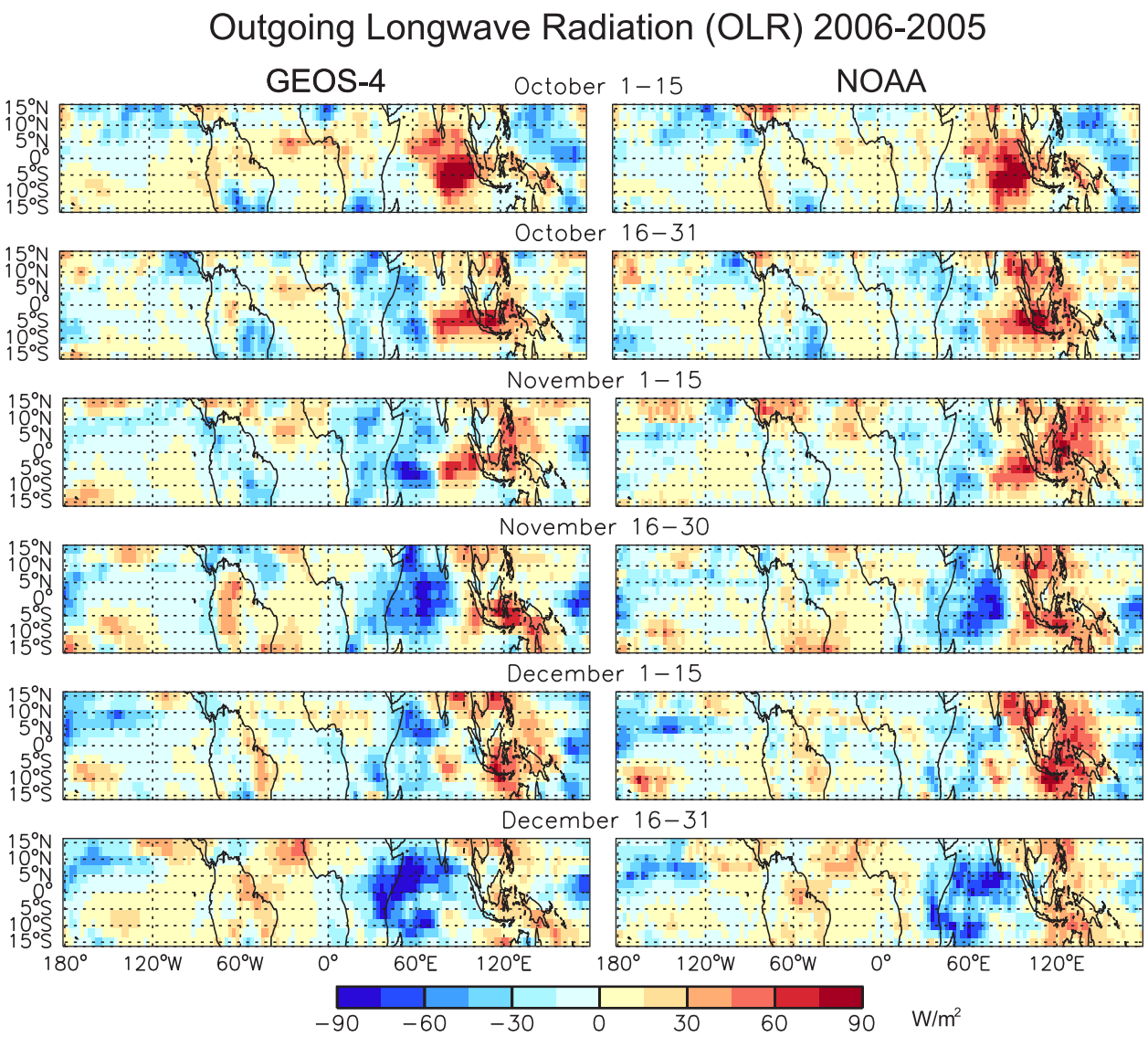

Figure 14: Differences in OLR (2006-2005) from GEOS-4 and NOAA for October to December in half-month intervals.

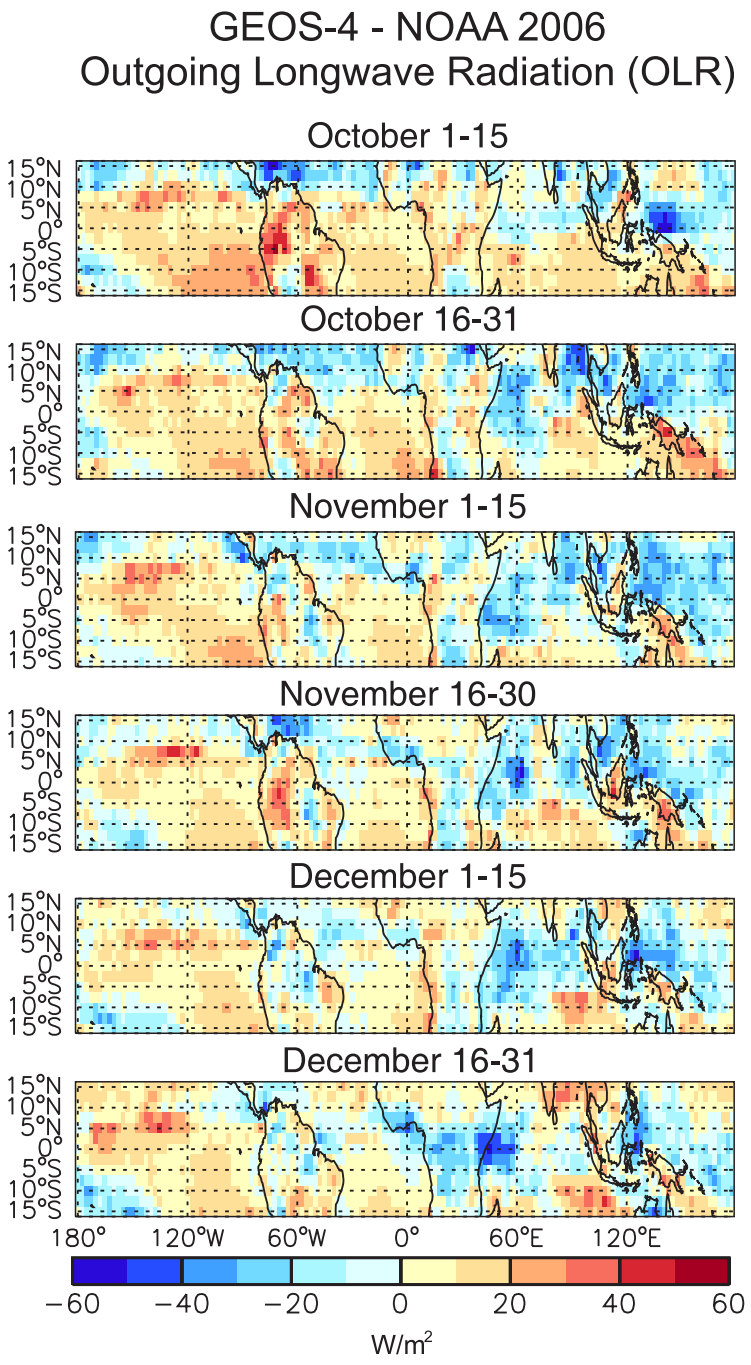

Figure 15: GEOS-4 – NOAA OLR for October to December 2006 after applying a bias correction of 13 W/m^2 to account for differences between the OLR datasets (see Figure 11).

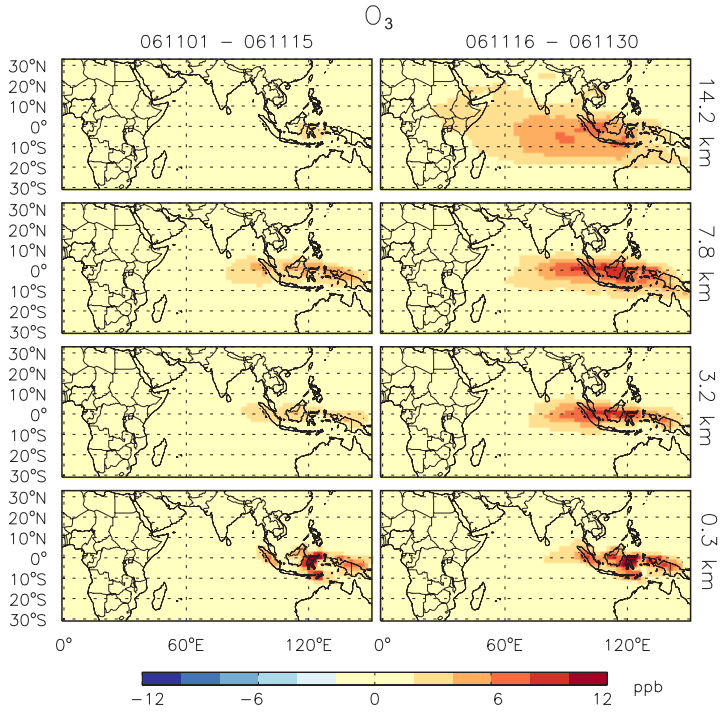

Figure 16: Ozone change resulting from an increase in soil NO_x emissions by a factor of 10, for the first and second halves of November near the base of the tropopause, UT, LT and BL. The change was calculated from the difference of *SoilNOx10 – Base*. Approximate altitudes corresponding to GEOS-4 sigma levels are given on the right.